Response to Reviewer's Comments

Manuscript Number: acp-2016-226

Authors: Junfeng Wang, Xinlei Ge, Yanfang Chen, Yafei Shen, Qi Zhang, Yele Sun, Jianzhong Xu, Shun, Ge, Huan Yu, Mindong Chen

Response to Reviewer #1 (Prof. Chen)

General comment: This manuscript reports the measurement results of submicron aerosols by the SPAMS in Nanjing. Recently the Aerodyne AMS has been widely used around the world, and this work presents for the first time the results using the SP-AMS in the YRD region. This is overall a very well written paper with quite thorough analyses of the data, the figures are informative and the results provide new insights regarding the aerosol chemistry in this region.

Authors' reply: We thank Prof. Chen for his positive comment.

Other comments:

As the paper is submitted to the PEEX special issue, it will be good for the authors to describe the link of the results presented in this work with the overall scientific goal of this special issue.

Authors' reply: As per the request, we have now added a sentence that describes the relationship of this work with PEEX, in the end of the introduction part, " *The findings for such a megacity are also valuable to the Pan-Eurasian Experiment (PEEX) infrastructure which aims to resolve the major uncertainties in Earth system science and global sustainability issues (Kulmala et al., 2015).*"

"A constant collection efficiency (CE) of 0.5 was used for the mass quantification, in consistent with many other AMS studies, as indeed the mass fraction of ammonium nitrate (mostly <40%), particle acidity (near neutral) and RH (<10%) do not affect the CE significantly for this dataset (Middlebrook et al., 2012)." It is a bit difficult for non-AMS users to understand this point. Consider rephrasing to make the statement clear.

Authors' reply: As requested by the reviewer and also the CE issue raised by referee #3, we have now elaborated this issue in the revised manuscript. "*A collection efficiency is typically used to account for the particles that are not measured by the instrument, due to the particles lost during passage through inlet, time-of-flight chamber and bouncing from the vaporizer. For the SP-AMS, the CE of laser vaporizer is mainly governed by particle divergence, while for the tungsten vaporizer, the CE is governed mainly by the bouncing effects (Matthew et al., 2008). An AMS CE*

value of 0.5 is typically valid and used commonly for most environments (Canagaratna et al., 2007). Nevertheless, Middlebrook et al. (2012) further found that high aerosol acidity, high ammonium nitrate mass fraction, and high sampling line RH could increase the CE, and provide a composition-dependent CE parameterization. For our dataset, we found that the composition-dependent CE rather than a constant CE=0.5 has negligible effects on the quantification of aerosol species, as the particles were neutralized (Fig. 3a), the mass fraction of ammonium nitrate were <40% in almost all cases, and also the sampling line RH was below 10%. In fact, the PM_1 mass concentrations by using the composition-dependent CE correlate a bit worse with the $PM_{2.5}$ concentrations than ones using CE=0.5. For these reasons, we chose the constant CE of 0.5, in consistent with many other AMS studies, for this dataset. "

In Fig.2, the authors used the $K_{p,AN}$ values to elucidate the formation mechanism of nitrate. Do the authors have gaseous NH_3 and HNO_3 data to make the argument more robust?

Authors' reply: Thanks for the suggestion. Unfortunately, we didn't have the co-located measurements of gaseous NH_3 and HNO_3, yet the theoretically estimated $K_{p,AN}$ values are likely adequate for illustrating the main formation pathway of nitrate.

In Fig.2b and Fig.10d, the authors separated the data into bins with 5ug/m3 increment, i think it will be better to make similar plots that describes the variations of aerosol compositions continuously against the mass loadings.

Authors' reply: As suggested, we have tried to re-plot the figure using all data instead of binned data. The new figures are shown below. However, due to the large amount and dramatic variations of the data, it is not easy to clearly observe the trends of particle compositions with the increase of PM_1 mass loadings; we thus kept the original plots in the new manuscript, as they seem to better help interpretation of the data.

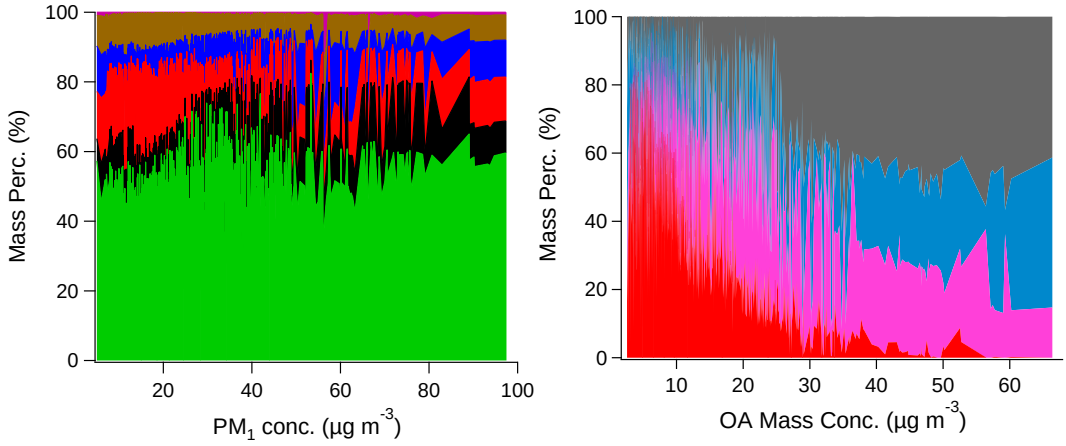

It is interesting to use polar plots to demonstrate the characteristics of organic aerosols. How about similar plots for the inorganic species?

Authors' reply: The aim of the polar plots is to qualitatively describe the spatial distribution of the different aerosol species. As suggested, we have added the polar plots for nitrate, sulfate and total OA in Fig. 11. As can be seen from the new Fig.11. SV-OOA has overall similar distribution with nitrate, again verifying its semi-volatile behavior, while both sulfate and LV-OOA have broader distributions, suggesting their features as regional species. Relevant text added in the revised manuscript, "*Nitrate, as a semi-volatile species, behaves overall similar to the SV-OOA. High concentrations of LV-OOA are distributed in all directions under higher WS, similar to that of sulfate, representing their regional behaviors.*"

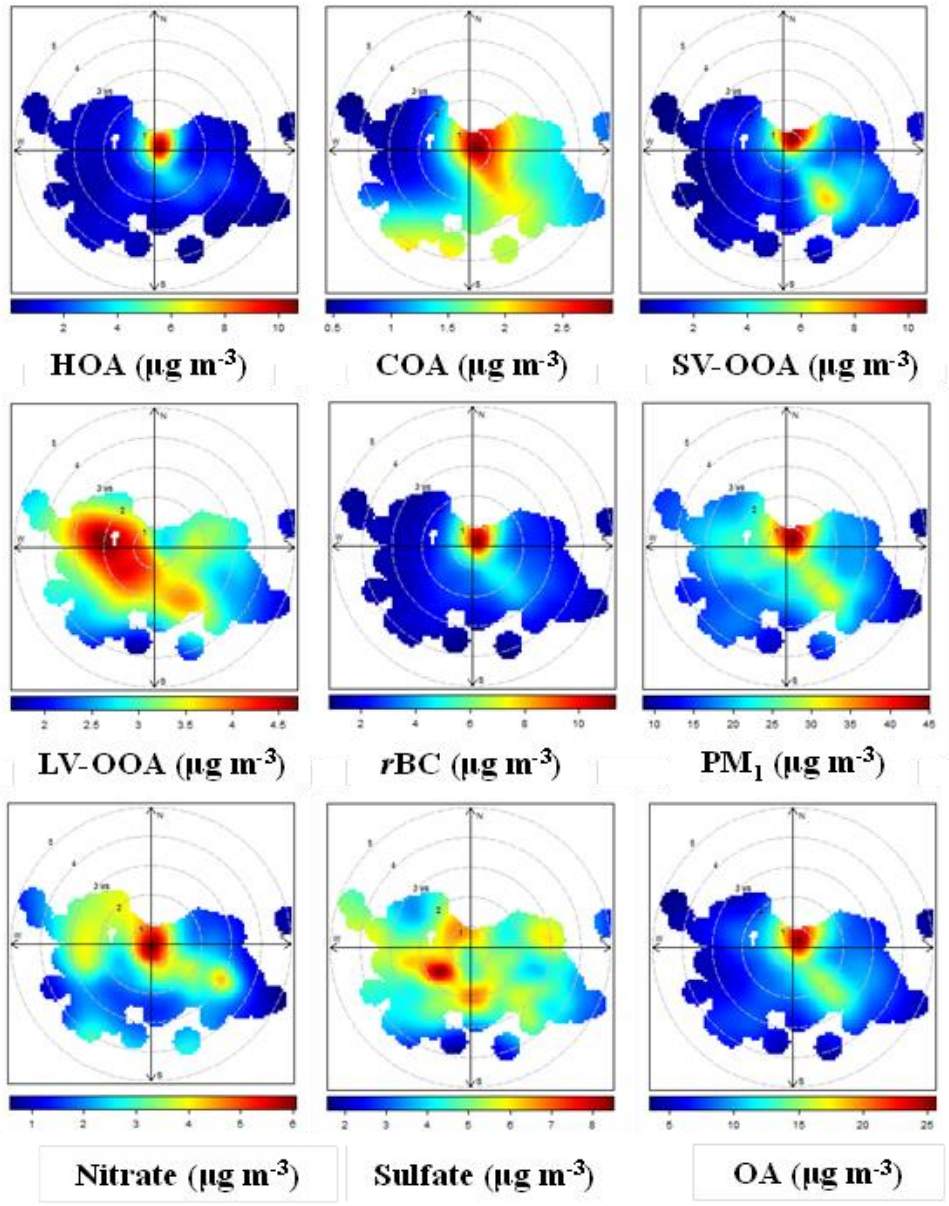

As the SP-AMS can measure both non-refractory and refractory species, it may provide unique information regarding the composition of refractory organics which cannot be measured by other AMS, this reviewers feel relevant discussion is lacking in the current manuscript.

Authors' reply: The reviewer perhaps didn't pay attention to Fig. 7, which compares the mass spectra obtained under dual-vaporizer setting and tungsten-only setting. It should be noted that, although under laser vaporization, some refractory organics can be detected, yet the SP-AMS cannot measure all refractory organics of the fine aerosols, but only the portion that is coated on *r*BC core. Overall, this portion seems to be negligible for this dataset, as can be seen in Fig. 7. We have also elaborate the discussion of this issue in the revised manuscript.

In Fig.12, the authors show the O/C vs. RH. Instead, i suggest to show the SV-OOA and LV-OOA mass concentrations with the increase of RH, so as to better demonstrate the influences of RH on the SOA formation.

Authors' reply: Thanks for the suggestion. We have added the plots which illustrate the SVOOA and LVOOA mass concentrations versus RH in the new manuscript. As shown below, both SVOOA and LVOOA mass concentrations don't increase with the increase of RH, the mass loading even start to decrease at high RH ranges, similar as the conclusions drawn from the O/C vs. RH plot, the results indicates insignificant influences from aqueous-phase oxidation for the SOA formation. Relevant text added in the revised manuscript, "*In addition, SV-OOA and LV-OOA mass concentrations, and O/C ratios of OA all show no obvious correlations with the RH as shown in Fig. 12b and Fig. 12c, indicating that aqueous-phase processing is insignificant compared to the photochemical processing for the oxidation of OA.*"

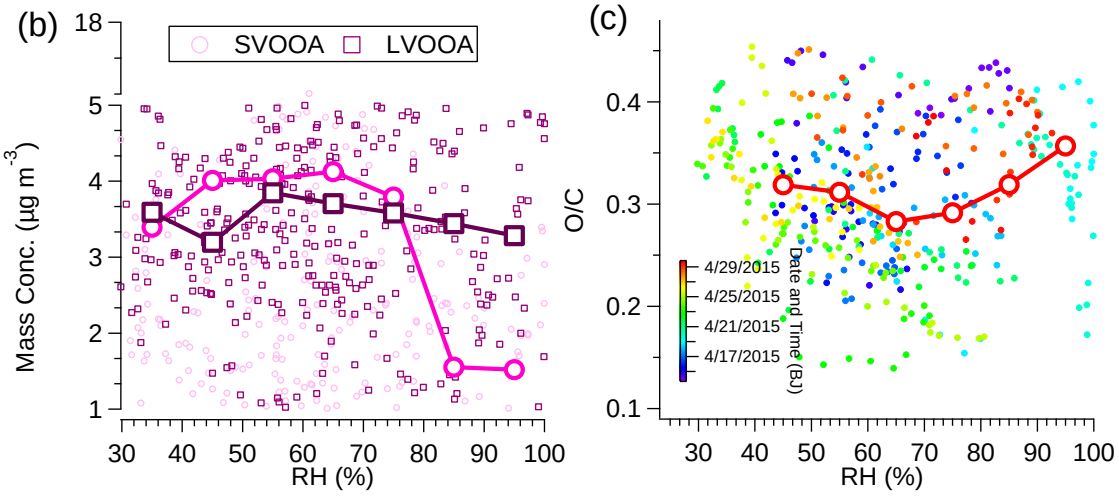

Response to Anonymous Referee #2

General Comment: The paper of Wang et al. describes the chemical characteristics of urban aerosol in Yangtze River Delta, China, measured by using a soot particle aerosol mass spectrometer. The results showed that most of the submicron particles consisted of organics, sulfate, nitrate, ammonium and black carbon. Authors used the results on chemical species to construct the light extinction, chemically resolved mass size distributions and the source apportionment of organics. Four factors were found for organic aerosol in Yangtze River Delta, hydrocarbon-like, cooking-related, semivolatile oxygenated and low-volatility oxygenated OA. Secondary OA dominated total organics, but when large OA concentrations were observed, the contribution of primary organics increased indicating the importance of anthropogenic sources.

This paper is well-written and the data have been analyzed and discussed very thoroughly. However, as there are so many AMS papers published on urban aerosols in past 15 years, it is difficult to see what is the significance and novelty of this paper. Are there any results presented in this paper that have not been published before? I suggest authors to think carefully what is the contribution of this paper to aerosol science and emphasize that clearly in the manuscript. Maybe it could be the unique features of the SP-AMS that allows to investigate the refractory material in addition to non-refractory species. In that case I suggest to focus this paper on that topic more clearly. This paper should be published after minor revision.

Authors' reply: We thank the referee for his/her overall positive comment on my work. Indeed, as a powerful tool for aerosol measurements, the AMS-related publications increased significantly in recent years. However, we believe that our results presented here are valuable and novel to the aerosol science: 1) Nanjing is one of the megacities in the densely populated Yangtze River delta region, but only two highly-time resolved studies using ACSM had been conducted during summer and winter for the aerosol characterization in Nanjing. Our study for the first time conducted the AMS measurement during springtime; 2) The ACSM cannot provide chemically-resolved size distribution of aerosol species, and cannot provide the HRMS of organic aerosols, while the high chemical resolution is sometimes critical for chemical speciation, and accurate source apportionment of OA; 3) ACSM cannot provide simultaneous measurement of BC. Overall, in this paper, we presented new data and new interpretation regarding the aerosol behaviors, sources and formation processes in Nanjing. These results are themselves never reported and insightful, enabling us to identify the diurnal patterns of different aerosol species, different sources that contribute to the aerosol mass, as well as the dominant pathway for the formation of secondary inorganic and organic aerosols, which are valuable for the abatement of

atmospheric pollution in China as well as in other megacities of the world. Relevant text was added in the introduction section, "*The rich highly-time resolved, highly-chemical resolved mass spectral data, as well as chemically-resolved size distributions of different aerosol species obtained for the first time in Nanjing during this study, can allow us to conduct in-depth analyses, and better understand the characteristics, sources and relevant transformation processes of ambient aerosols in Nanjing. The findings for such a megacity are also valuable to the Pan-Eurasian Experiment (PEEX) infrastructure which aims to resolve the major uncertainties in Earth system science and global sustainability issues (Kulmala et al., 2015)*."

Indeed, it is a unique feature that the SP-AMS is able to measure some refractory organics that other types of AMS cannot measure. We have added relevant discussion in Section 3.2, "*It should be noted that, accurate determination of refractory organics is very difficult, because: 1) A large portion of refractory organics cannot be detected by the SP-AMS if they didn't coat on rBC cores; 2) To accurately measure the species only coated on rBC cores, the tungsten vaporizer has to be physically removed, otherwise the vaporizer temperature is still around 150oC even its power is turned off, and the non-refractory organics that don't coat on rBC cores can still be measured, and complicates the analyses; 3) The CE and IE values for different species may vary under different vaporizer settings, so that direct subtraction of organics measured under tungsten-only setting from the organics measured under dual-vaporizer setting may not represent the real refractory organics; 4) Some ions measured under dual-vaporizer setting are likely induced by the laser itself rather than the 70 ev electron impact. For example, a series of fullerene-like carbon clusters can be generated by the laser itself, even though they don't really exist in the atmosphere (Wang et al., 2016;Onasch et al., 2015). This laser-induced ion formation scheme may work for other organics, thus makes it even more difficult for identifying the refractory organics. Further studies are essential to investigate this issue."* Moreover, we think this issue might be further explored by using a laser-only SP-AMS in parallel with a HR-AMS, and other instruments such as SP2, etc., for the specifically-designed chamber simulations that using *r*BC as seed aerosols, or for the real atmospheric environment where the *r*BC is heavily coated and internally mixed with other species. For this campaign, since we only have one SP-AMS without other supporting data, we are unable to conduct such in-depth investigations; in fact, we expect to elaborate this issue in more details in another publication as we had conducted such a campaign having HR-AMS, laser-only SP-AMS and other *r*BC instruments together, in Tibet.

Specific comments:

1. Page 2, line 34: remove (_54% of the PM2.5 mass) unimportant detail.

Authors' reply: Done

2. Page 5, line 124: Why springtime? Is there something specific in aerosol chemistry in springtime Yangtze River Delta? Add a reason for springtime measurements.

Authors' reply: During summertime, there may be influences from biomass burning and aqueous-phase oxidation, and during wintertime, there may be heating-related emissions in Nanjing. During springtime, the aerosol sources are likely different, yet there are no springtime AMS studies conducted before to probe the aerosol characteristics. Indeed, in this study, we found no influences from biomass burning, and coal-burning related factors, showing the different behaviors of springtime aerosols from those in other season. This has been stated clear in the introduction part of the revised manuscript now. "*Moreover, none of the previous AMS measurements studied the aerosol characteristics during springtime in Nanjing, yet the springtime aerosols may have different behaviors than those in other seasons, when aerosols are likely influenced significantly by emissions from biomass burning, coal burning etc.*" In addition, we chose to conduct the measurement in the specific urban site is to help resolve the sources of aerosols in that site, as previous monitoring data shows a bit higher $PM_{2.5}$ level than those from adjacent sites. Thus, the findings in this paper also serve to the policy making of the local environmental protection agency.

3. Page 6, line 148: "coated species" Specify. What are the core and what are the coating species?

Authors' reply: Here, the "coated species" refer to the inorganic and organic components that coated on the *r*BC cores. It has been added in the revised manuscript.

4. Page 7: lines 183-186: collection efficiency, how is CE defined for the SP-AMS? Discuss with relevant citation.

Authors' reply: The CE issue is now elaborated in the revised manuscript. Please refer to the reply to reviewer #1.

5. Page 8, 206-210: no difference in OA factors between dual vaporizer and tungsten vaporizer; how about rBC? With dual vaporizer set-up you are able to separate rBC for different PMF factors. It would have been interesting to see how rBC divides between HOA and COA, or does it?

Authors' reply: We thank the referee for pointing out this question as we didn't state it clearly. Here, in this paper, we focused on the sources or non-refractory organics, thus we conducted PMF on the organics obtained under tungsten-only setting. We have also conducted PMF analyses on the organics obtained under dual-vaporizer setting but without including the *r*BC. As

shown in Fig.7, the organics mass spectra (with no *r*BC) are quite similar for these two circumstances, and we indeed found no significant difference from the PMF factors.

6. Page 17 and Fig 9; I suggest rather showing the correlation (time-series) of PMF factors and inorganic species than PMF factors and organic tracers in Figure 9.
Authors' reply: We now added the time series of nitrate and sulfate in Fig. 9.

7. Page 35, Figure 5a: Is it possible that the right side of the mass size distributions is defined by the transmission of aerodynamic lens? Could you estimate how much of the accumulation mode mass is missing for organics, sulfate, nitrate, ammonium and chloride because of that?

Authors' reply: The reviewer is correct. AMS has different transmission efficiencies for particles with different sizes due to the inlet system. Fluid dynamic simulation of the AMS inlet shows that the AMS shows 100% transmission efficiency for 70-500nm particles, and substantial transmission for small particles (30-70nm) and large particles (500nm-2.5μm) for spherical particles (Jayne et al., 2000). The AMS is referred to as a PM_1 instrument, as its transmission efficiency at 1μm is approximately 50%. Recently, there is a new lens system that can efficiently transmit supermicron particles up to 3 μm (Williams et al., 2013), but instead its transmission efficiency for small particles (left side) was significantly decreased.
Overall it is very difficult to estimate how much of the mass is missing due to the incomplete transmission of our SP-AMS inlet system. A possible way is to inject the DMA-selected monodisperse single-component particles (pure ammonium nitrate, ammonium sulfate, ammonium chloride, etc), and compares the AMS-measured numbers with the particle numbers counted by the CPC – however, this method is also limited by the upper size cut of the DMA (typically ~700 nm), and also there is no proper reference material for the estimation of organics. Nevertheless, the AMS is able to capture the bulk of ambient accumulation mode particles in the submicron meter range, relevant discussion and analyses mainly focus on the peak modes in PM_1 range as well. We have added a sentence to elaborate this point in section 3.2, "*It also should be note that, although the AMS is able to capture the bulk of atmospheric accumulation mode particles (Canagaratna et al., 2007), right side of size distributions may be affected by the incomplete transmission of larger particles limited by the SP-AMS inlet (in particular, the supermicron ones).*"

Technical corrections:
Page 3, lines 67-68: parenthesis are used unclearly

Page 15, line 428: …the SV-OOA… remove "the" as you haven't used it with PMF factors earlier

Authors' reply: Corrected.

Response to Anonymous Referee #3

General comments: The paper deals with highly time-resolved urban aerosol characterization during two weeks period in spring in Nanjing (China) using soot particle high resolution aerosol mass spectrometry. The work makes use of most possibilities that SP HR-AMS gives and the whole text is clearly written using good English. Although the topic is important, there are several major issues that should be answered before publishing the paper.

Authors' reply: We thank the referee for his/her overall positive comment on my work, and we have tired our best to address the specific comments below.

First, although the use of collection efficiency 0.5 was common in the past, nowadays a composition dependent collection efficiency (Middlebrook et al., 2012) should be used or at least tested as a composition is highly variable during sampling, as seen on diurnal variability of major species. This is even more important when no reference data for comparison with AMS total mass or any species are present. Second, as automatic using of CE equal 0.5 induces higher uncertainty for determination of PM1 mass, it should be stated when it is compared to PM2.5 mass. The average ratio PM1 to PM2.5 equal to 0.54 is rather low especially when relatively low (for China) average concentrations were present during sampling period and at the same time average RH was not high.

Authors' reply: As also requested by reviewer #1, we have now elaborated this issue in the revised manuscript. "*A collection efficiency is typically used to account for the particles that are not measured by the instrument, due to the particles lost during passage through inlet, time-of-flight chamber and bouncing from the vaporizer. For the SP-AMS, the CE of laser vaporizer is mainly governed by particle divergence, while for the tungsten vaporizer, the CE is governed by the bouncing effects (Matthew et al., 2008). An AMS CE value of 0.5 is typically valid and used commonly for most environments (Canagaratna et al., 2007). Nevertheless, Middlebrook et al. (2012) further found that high aerosol acidity, high ammonium nitrate mass fraction, and high sampling line RH could increase the CE, and provide a composition-dependent CE parameterization. For our dataset, we found that the composition-dependent CE rather than a constant CE=0.5 has negligible effects on the quantification of aerosol species, as the particles*

were neutralized (Fig. 3a), the mass fraction of ammonium nitrate were <40% in almost all cases, and also the sampling line RH was below 10%. In fact, the PM_1 mass concentrations by using the composition-dependent CE correlate a bit worse with the $PM_{2.5}$ concentrations than ones using CE=0.5. For these reasons, we chose the constant CE of 0.5, in consistent with many other AMS studies, for this dataset."

In addition, the measured ratio of 0.54 for PM_1 to $PM_{2.5}$ seems a bit low, but is close to 0.63 for PM_1 to $PM_{2.5}$ measured by the ACSM during Nanjing Winter by Zhang et al. (2016), and higher than 0.38 measured by the HR-AMS during Lanzhou Summer by Xu et al. (2014). We have added a sentence to state clearly the uncertainty due to CE of the SP-AMS. "*This ratio appears to be a bit low, likely due to the uncertainty of CE of the SP-AMS*."

Next, although using oxidation ratio of sulphur probably makes sense, the similar ratio for nitrogen (line 266) has no meaning as gas phase nitric acid is not included and there are also other nitrogen oxides than NO2 that are not accounted for. The explanations about mainly photochemical origin of sulphate (lines 271-275) is misleading, the ratio SO42-/NO3- has nothing to do with sulphate origin. At the same time, although the maximum in oxidation ratio of sulphur in the afternoon may suggest influence of photochemical oxidation of SO2, it does not prove it. The same effect can be expected during increased mixed boundary layer period from down mixing of older aerosol from upper boundary layer in which the most of SO2 was oxidized some time ago. The size distribution of sulphate presented in Fig. 5 actually supports liquid phase formation of sulphates (Hering and Friedlander 1982).

Authors' reply: Thanks for pointing out this issue. We agree with the reviewer that due to possible existence of other nitrogen oxides and gaseous nitric acid, the f_N defined here may be not a good proxy to represent the oxidation of NO_2, so we have now removed Fig.4b, 4c, 4e and 4f. Instead, we added one plot that depicts the relationship of nitrate and sulfate concentrations with RH. From Fig. 4b and 4c, we can find that the f_s shows anti-correlation with the RH, and also, the mass concentrations of sulfate don't show clearly positive correlation with the RH – the mass loadings even start to drop under high RH conditions. We postulate that at least it suggests that aqueous-phase oxidation doesn't show significant influence on sulfate formation. Indeed, we cannot completely exclude the possibility that increase of f_s or sulfate during afternoon might be due to down mixing of sulfate that formed some time ago. However, on the other hand, as all aerosol species are mixed together, the down mixing effect may have also increased the concentrations of other species as well - which was indeed observed before in Lanzhou summer (Xu et al., 2014). Yet concentrations of all other species, on the contrary, decreased significantly

during afternoon. We thus think these behaviors suggest that the afternoon photochemical formation of sulfate is likely dominant rather than the aqueous-phase processing. The size distributions data may have limited use here for describing the formation pathway of sulfate or nitrate - as all secondary inorganic species peak in a similar mode size around 500-700nm (the peak size of nitrate even appears to be a bit larger than that of sulfate).

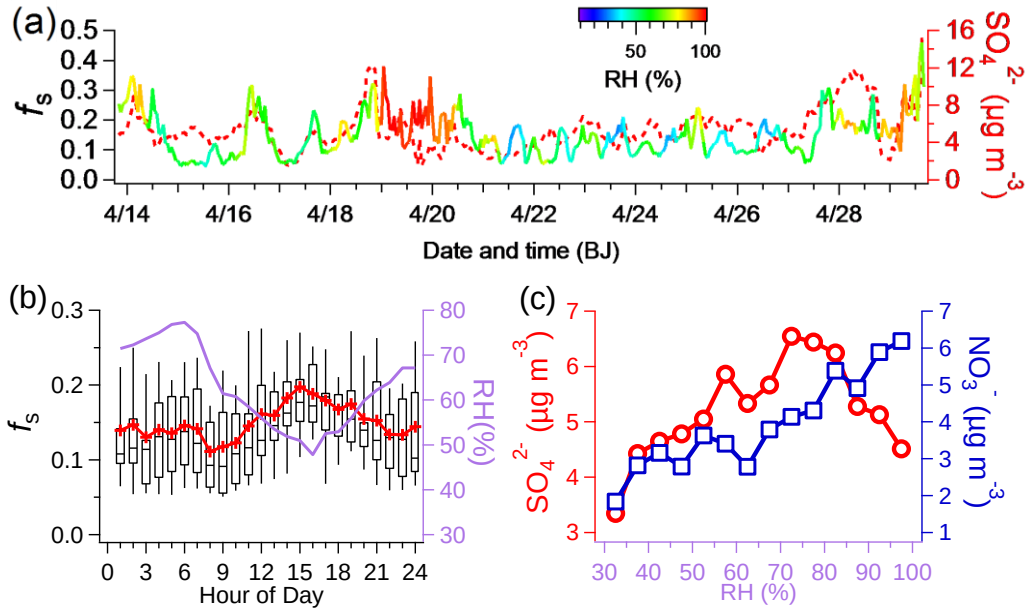

The text regarding Fig. 4 is now re-written. "*In order to further elucidate the formation processes of sulfate, we calculated the oxidation ratios of sulfur (f_S) (Fig. 4a), defined as $f_S = nSO_4^{2-}/(nSO_4^{2-} + nSO_2)$ (Xu et al., 2014), indicating the conversion of SO_2 . Here nSO_4^{2-} and nSO_2 are the molar quantities of particle-phase sulfate, and gas-phase SO_2, respectively. Diurnal variations of f_S and RH are presented in Fig.4b, and Fig. 4c shows variations of sulfate and nitrate concentrations with RH. The diurnal profile of f_S shows a negative correlation with that of RH (r = -0.52), and mass concentrations of sulfate even drop under high RH conditions, indicating somewhat an insignificant role of aqueous-phase process for sulfate formation during this campaign. On the other hand, the f_S reaches a maximum around 3 pm. Note the afternoon rise of fs and sulfate may be affected by the down mixing of sulfate formed earlier, however, since concentrations of all other aerosol species that mix with sulfate decrease significantly, we postulate that the increase of fs likely suggest the photochemical production of sulfate in the afternoon.*"

The source apportionment as presented here is not very clear. The decision why the authors use four and not five factors seems little subjective. At the same time high correlation of "SV-OOA"

factor with rBC, CO and NO2 (very similar to HOA factor) together with its very local origin (Fig. 11) does not seem to agree with its secondary origin. The doubts about SV-OOA in this work are also confirmed in the text and Table 1 because of its low correlation with SV-OOA from two other cities in China. The reviewer suggests testing five factor solution more thoroughly.

Authors' reply: Sorry that we didn't put enough details regarding the choice of PMF factors. In fact, we have investigated the 5-factor solution space carefully before choosing 4-factor one as the best solution. 1) 4-factor SVOOA mass spectrum does correlate a bit worse with the SVOOA from Beijing and Lanzhou, compared with the correlation coefficients of other factors. But it does correlate very well with the OOA from Fresno. Further investigation finds that the relative weak correlation (r^2= 0.75) between 4-factor SVOOA with Beijing SVOOA is mainly due to 3 ions, CO_2^+, CO^+ and H_2O^+ (in theory, only CO_2^+, as the other two ions are scaled to CO_2^+); and if we exclude these 3 ions, r^2 will be 0.88. Similarly, the weaker correlation with Lanzhou SVOOA is mainly due to $C_2H_3O^+$, if we excluded this ion, r^2 will be 0.89. These results suggest that the 4-factor SVOOA MS is in consistent with previous studies.

2）Correspondingly, although correlations between factor 2 of 5-factor solution ("SVOOA" in 5-factor solution) with Beijing and Lanzhou SVOOA does improve a little than "SVOOA" in 4-factor solution (r^2=0.72 vs. 0.68 with Beijing, and r^2=0.80 vs. 0.75 with Lanzhou), the correlation with Fresno OOA on the other hand, becomes a bit worse (r^2= 0.87 vs. 0.91). Thus we think there is no specific reason to conclude that the SVOOA in 5-factor solution is better than the SVOOA in 4-factor solution, at least based on the spectral similarity.

3) "SVOOA" in 5-factor solution almost has no correlation with nitrate (r=0.07), while the SVOOA in 4-factor solution correlates relatively well with nitrate (r=0.49).

4) Factor 4 in 5-factor solution is hard to explain. It is not BBOA because of negligible signals at m/z 60 and 73. Its spectrum is not similar to HOA (r^2=0.33, 0.24 and 0.26 with HOA of Beijing, Lanzhou and Fresno), COA (r^2= 0.27, 0.39 and 0.40 with COA of Beijing, Lanzhou and Fresno), or SVOOA (r^2=0.42 and 0.48 with SVOOA of Beijing and Lanzhou).

5) Factor 4 and Factor 2 in the 5-factor solution seems to be a split of SVOOA in 4-factor solution. First, the O/C of 0.32 of SVOOA in 4-factor solution is between 0.28 of Factor 4 and 0.42 of Factor 2 in the 5-factor solution; more importantly, if we combined Factor 2 and Factor 4 into one "Combined factor", its time series correlate very well with the SVOOA in 4-factor solution (r^2=0.89) with a slope of 1.05, suggesting clearly the factor splitting.

（6）Our results do suggest that SVOOA is locally formed, it has good correlations with rBC, and HOA. We think this does not necessarily mean that the PMF is not correct, or the SVOOA we separate is in fact a primary OA factor. More likely, it is a locally formed fresh SOA, which

derived from the in-situ fast oxidation of traffic or cooking VOCs. Of course, this issue requires more careful investigation.

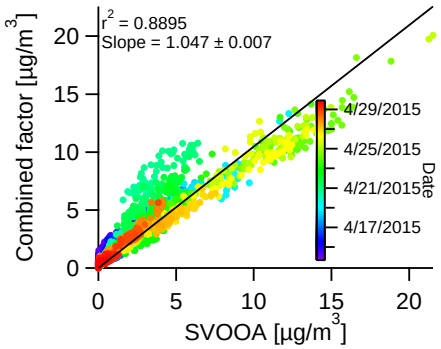

We have added some discussions into the revised manuscript. "*Following the instruction detailed by Zhang et al. (2011), the 4-factor solution (at fpeak = -0.1) was chosen as the optimal solution, as the 3-factor solution cannot separate the hydrocarbon-like OA (HOA) and cooking OA (COA) (Fig. S2). For the 5-factor solution (Fig. S3), Factor 2 and Factor 4 are clearly a split from the SVOOA from the 4-factor solution (r2 = 0.89 and slope of 1.05); Factor 2 of 5-factor solution also shows much weaker correlations with nitrate than SVOOA of 4-factor solution does (r = 0.07 vs. 0.49).*"

The text in lines 457-460 at least partially contradicts the conclusions based on Van Krevelen diagram.

Authors' reply: Thanks for pointing out this issue. We have modified the relevant discussion for the Van Krevelen diagram. The VK diagram should be used with cautions as for ambient data it cannot exclude mixing effects. The data follows a line with a slope of -1 may not reflect the real aging mechanism is the addition of carboxylic acid. We thus delete the statement "the propagation of OA is similar to an aging process that is likely driven by the addition of carboxylic acid (slope of -1)".

More attention should be paid to the differences between dual vaporizer and a tungsten vaporizer data, as it can bring more light on the influence of refractory organics.

Authors' reply: We thank the referee for his/her suggestion. We have added some discussion regarding this issue. Please check the reply to reviewer #2.

The corrections and doubts described above should be also corrected in the Abstract (e.g. lines 54-55) and the Conclusions (lines 545, 553-554, 561-574).

Authors' reply: We have modified accordingly the Abstract and Conclusions in the revised manuscript.

References

Canagaratna, M. R., Jayne, J. T., Jimenez, J. L., Allan, J. D., Alfarra, M. R., Zhang, Q., Onasch, T. B., Drewnick, F., Coe, H., Middlebrook, A., Delia, A., Williams, L. R., Trimborn, A. M., Northway, M. J., DeCarlo, P. F., Kolb, C. E., Davidovits, P., and Worsnop, D. R.: Chemical and microphysical characterization of ambient aerosols with the aerodyne aerosol mass spectrometer, Mass Spectrom. Rev., 26, 185-222, 10.1002/Mas.20115, 2007.

Jayne, J. T., Leard, D. C., Zhang, X., Davidovits, P., Smith, K. A., Kolb, C. E., and Worsnop, D. R.: Development of an Aerosol Mass Spectrometer for Size and Composition Analysis of Submicron Particles, Aerosol Sci. Tech., 33, 49 - 70, 10.1016/S0021-8502(98)00158-X, 2000.

Kulmala, M., Lappalainen, H. K., Petäjä, T., Kurten, T., Kerminen, V. M., Viisanen, Y., Hari, P., Sorvari, S., Bäck, J., Bondur, V., Kasimov, N., Kotlyakov, V., Matvienko, G., Baklanov, A., Guo, H. D., Ding, A., Hansson, H. C., and Zilitinkevich, S.: Introduction: The Pan-Eurasian Experiment (PEEX) – multidisciplinary, multiscale and multicomponent research and capacity-building initiative, Atmos. Chem. Phys., 15, 13085-13096, 10.5194/acp-15-13085-2015, 2015.

Matthew, B. M., Middlebrook, A. M., and Onasch, T. B.: Collection Efficiencies in an Aerodyne Aerosol Mass Spectrometer as a Function of Particle Phase for Laboratory Generated Aerosols, Aerosol Sci Tech, 42, 884-898, 10.1080/02786820802356797, 2008.

Middlebrook, A. M., Bahreini, R., Jimenez, J. L., and Canagaratna, M. R.: Evaluation of Composition-Dependent Collection Efficiencies for the Aerodyne Aerosol Mass Spectrometer using Field Data, Aerosol Sci. Tech., 46, 258-271, 10.1080/02786826.2011.620041, 2012.

Onasch, T. B., Fortner, E. C., Trimborn, A. M., Lambe, A. T., Tiwari, A. J., Marr, L. C., Corbin, J. C., Mensah, A. A., Williams, L. R., Davidovits, P., and Worsnop, D. R.: Investigations of SP-AMS Carbon Ion Distributions as a Function of Refractory Black Carbon Particle Type, Aerosol Sci. Tech. , 49, 409-422, 10.1080/02786826.2015.1039959, 2015.

Wang, J., Onasch, T. B., Ge, X., Collier, S., Zhang, Q., Sun, Y., Yu, H., Chen, M., Prévôt, A. S. H., and Worsnop, D. R.: Observation of Fullerene Soot in Eastern China, Environmental Science & Technology Letters, 3, 121-126, 10.1021/acs.estlett.6b00044, 2016.

Williams, L. R., Gonzalez, L. A., Peck, J., Trimborn, D., McInnis, J., Farrar, M. R., Moore, K. D., Jayne, J. T., Robinson, W. A., Lewis, D. K., Onasch, T. B., Canagaratna, M. R., Trimborn, A., Timko, M. T., Magoon, G., Deng, R., Tang, D., de la Rosa Blanco, E., Prévôt, A. S. H., Smith, K. A., and Worsnop, D. R.: Characterization of an aerodynamic lens for transmitting particles greater than 1 micrometer in diameter into the Aerodyne aerosol mass spectrometer, Atmos. Meas. Tech., 6, 3271-3280, 10.5194/amt-6-3271-2013, 2013.

Xu, J., Zhang, Q., Chen, M., Ge, X., Ren, J., and Qin, D.: Chemical composition, sources, and processes of urban aerosols during summertime in northwest China: insights from high-resolution aerosol mass spectrometry, Atmos. Chem. Phys., 14, 12593-12611, 10.5194/acp-14-12593-2014, 2014.

Zhang, Q., Jimenez, J., Canagaratna, M., Ulbrich, I., Ng, N., Worsnop, D., and Sun, Y.: Understanding atmospheric organic aerosols via factor analysis of aerosol mass spectrometry: a review, Anal. Bioanal. Chem., 401, 3045-3067, 10.1007/s00216-011-5355-y, 2011.

Zhang, Y. J., Tang, L., Yu, H., Wang, Z., Sun, Y., Qin, W., Chen, W., Chen, C., Ding, A., Wu, J., Ge, S., Chen, C., and Zhou, H.-c.: Chemical composition, sources and evolution processes of aerosol at an urban site in Yangtze River Delta, China during wintertime, Atmos. Environ., 123, 339-349, 10.1016/j.atmosenv.2015.08.017, 2016.

Highly time-resolved urban aerosol characteristics during springtime in Yangtze River Delta, China: Insights from soot particle aerosol mass spectrometry

Junfeng Wang,[1] Xinlei Ge,[1,*] Yanfang Chen,[1] Yafei Shen,[1] Qi Zhang,[1,2] Yele Sun,[3] Jianzhong Xu,[4] Shun, Ge,[5] Huan Yu,[1] Mindong Chen[1,*]

[1]Jiangsu Key Laboratory of Atmospheric Environment Monitoring and Pollution Control (AEMPC), Collaborative Innovation Center of Atmospheric Environment and Equipment Technology (CIC-AEET), School of Environmental Science and Engineering, Nanjing University of Information Science & Technology, Nanjing 210044, China

[2]Department of Environmental Toxicology, University of California at Davis, Davis, California 95616, United States

[3]State Key Laboratory of Atmospheric Boundary Layer Physics and Atmospheric Chemistry, Institute of Atmospheric Physics, Chinese Academy of Sciences, Beijing 100029, China

[4]State Key Laboratory of Cryospheric Sciences, Cold and Arid Regions, Environmental and Engineering Research Institute, Chinese Academy of Sciences, Lanzhou 730000, China

[5]Nanjing Tianbo Environmental Technology Co., Ltd, Nanjing 210047, China

*Corresponding author, Email: caxinra@163.com; chenmdnuist@163.com

Phone: +86-25-58731394

For *Atmos. Chem. Phys.*

Abstract: In this work, the Aerodyne soot particle – aerosol mass spectrometer (SP-AMS) was deployed for the first time during the spring of 2015 in urban Nanjing, a megacity in the Yangtze River Delta (YRD) of China, for online characterization of the submicron aerosols (PM_1). The SP-AMS enables real-time and fast quantification of refractory black carbon (*r*BC) simultaneously with other non-refractory species (ammonium, sulfate, nitrate, chloride and organics). The average PM_1 concentration was found to be 28.2 μg m^{-3}~~, (~54% of the $PM_{2.5}$ mass),~~ with organics (45%) as the most abundant component, following by sulfate (19.3%), nitrate (13.6%), ammonium (11.1%), *r*BC (9.7%) and chloride (1.3%). These PM_1 species together can reconstruct ~44% of the light extinction during this campaign based on the IMPROVE method. Chemically-resolved mass-based size distributions revealed that small particles especially ultrafine ones (<100 nm vacuum aerodynamic diameter) were dominated by organics and *r*BC, while large particles had significant contributions from secondary inorganic species. Source apportionment of organic aerosols (OA) yielded four OA subcomponents, including hydrocarbon-like OA (HOA), cooking-related OA (COA), semi-volatile oxygenated OA (SV-OOA), and low-volatility oxygenated OA (LV-OOA). Overall, secondary organic aerosol (SOA, equal to the sum of SV-OOA and LV-OOA) dominated the total OA mass (55.5%), but primary organic aerosol (POA, equal to the sum of HOA and COA) can outweigh SOA in early morning and evening due to enhanced human activities. High OA concentrations were often associated with high mass fractions of POA and *r*BC, indicating the important role of anthropogenic emissions during heavy pollution events. The diurnal cycles of nitrate, chloride and SV-OOA both showed good anti-correlations with air temperatures, suggesting their variations were likely driven by thermodynamic equilibria and gas-to-particle partitioning. On the other hand, in contrast to other species, sulfate and LV-OOA concentrations increased during afternoon, and showed no positive correlations with relative humidity (RH), likely indicating the contribution from ~~the significant role of~~ photochemical ~~processing~~ oxidation is more important ~~rather~~ than that of aqueous-phase processing for their formations. The bivariate polar plots show

that the SV-OOA was formed locally, and the variations of hydrogen-to-carbon (H/C) and oxygen-to-carbon (O/C) ratios in the Van Krevelen space further suggests an evolution pathway of SV-OOA to LV-OOA. Our findings regarding springtime aerosol chemistry in Nanjing may have important implications for the air quality remediation in the densely populated regions.

1. Introduction

In recent years, high concentrations of fine particulate matter ($PM_{2.5}$) have been frequently observed (Hu et al., 2015), in accompanying with the visibility impairment and occurrence of haze events across large parts of China. $PM_{2.5}$ also affects human health (e.g., Pope and Dockery, 2006;Cao et al., 2012), regional and global climate (directly by absorbing and scattering solar radiation or indirectly by acting as cloud condensation nuclei and ice nuclei)(e.g.,Ghan and Schwartz, 2007;Pöschl, 2005), and the earth's ecosystem (Carslaw et al., 2010). These effects are predominantly dependent upon the physical and chemical characteristics of fine particles, such as mass concentration, chemical composition, size distribution, and hygroscopicity, all of which are influenced by the emission sources and transformation and evolution processes in the atmosphere.

The Yangtze River Delta (YRD) region is one of the most populated and economically developed areas in China, but it is also facing with severe air pollution lately. Nanjing, as one of the major megacities in this region, has a daily $PM_{2.5}$ mass concentration varying between 33-234 μg m^{-3} during November 2011 - August 2012, with an mean value of 106 μg m^{-3}, which is 4.2 times the WHO air quality standard of 25 μg m^{-3} (Shen et al., 2014). $PM_{2.5}$ pollution is significantly elevated during hazy days, for example, a daily average of 282 μg m^{-3} was observed for a heavily polluted day (Fu et al., 2008). A number of studies regarding aerosol chemistry in Nanjing have been conducted, and identified various inorganic components (sulfate, nitrate, ammonium and heavy metals, etc.) (e.g., Wang et al., 2003;Hu et al., 2012;Qi et al., 2016) and hundreds of organic species (carboxylic/dicarboxylic acids, amines and

amino acids, polycyclic aromatic hydrocarbons, etc.) (Wang et al., 2011;Wang et al., 2002;Yang et al., 2005;Wang et al., 2009) that contribute to the aerosol mass. However, past studies mostly employed filter-based sampling technique, which due to low time resolution (a few hours to days), is often incapable of capturing details of the atmospheric evolution processes during the typical lifecycle of aerosols (Wexler and Johnston, 2008). Subsequent offline analyses may also introduce artifacts as some semi-volatile species can evaporate during sampling and storage (Dong et al., 2012).

On the other hand, in the past 15 years, the Aerodyne Aerosol Mass spectrometer (AMS) (Canagaratna et al., 2007) has been widely used, and was proven to be powerful for real-time online measurements of size-resolved chemical compositions of submicron aerosols (PM_1) with very fine time resolution (seconds to minutes) (Zhang et al., 2007a;Jimenez et al., 2009). The development of Aerodyne AMS began with the invention of quadruple AMS (Q-AMS) (Jayne et al., 2000), following by the compact time-of-flight AMS (C-ToF-AMS) (Drewnick et al., 2005), high resolution time-of-flight AMS (HR-ToF-AMS) (DeCarlo et al., 2006) and the soot particle AMS (SP-AMS) (Onasch et al., 2012). There are also an aerosol chemical speciation monitor (ACSM) (Ng et al., 2011) and its updated version of ToF-ACSM (Fröhlich et al., 2013), which are in particular designed for long-term unattended aerosol measurements. SP-AMS is the most advanced version, which in principle incorporates the single particle soot photometer (SP2) into the HR-ToF-AMS, and upgraded with a laser vaporizer for detecting refractory black carbon (*r*BC) and associated/coated species that cannot be measured by other types of AMS.

Recently, the Aerodyne AMS has been deployed widely in China (particularly Beijing) (e.g., Xu et al., 2014 and references therein;Sun et al., 2014;Yeung et al., 2014;Zhang et al., 2014;Li et al., 2015;Shen et al., 2015;Sun et al., 2015a;Sun et al., 2015b;Yan et al., 2015;Zhang et al., 2015;Tang et al., 2016;Zhang et al., 2016a;Jiang et al., 2015;Chen et al., 2015;Xu et al., 2015;Du et al., 2015;Sun et al., 2016;Wang et al., 2015;Han et al., 2015;Wang et al., 2016b). However, only a few field campaigns were conducted in the YRD region. Huang et al. (2012b) deployed an HR-ToF-AMS

together with an SP2 in Shanghai during the 2010 Shanghai World Expo, and in Jiaxing during summer and winter of 2010 (Huang et al., 2012a). In urban Nanjing, an ACSM was applied for characterizing PM_1 during summer and autumn harvest seasons (Zhang et al., 2015), and during December 2013 to investigate a few heavy haze events (Zhang et al., 2016b). In addition, a Q-AMS was deployed in Nanjing to investigate the effects of PM_1 on visibility during January 2013 (Shen et al., 2015). Furthermore, a recent study by Wang et al. (2016a) reported the observation of fullerene soot in suburban Nanjing using an SP-AMS. Nevertheless, many questions remain unclear with regard to aerosol chemistry, sources, and processes in this region. Moreover, none of the previous AMS measurements studied the aerosol characteristics during springtime in Nanjing, yet the springtime aerosols may have different behaviors than those in other seasons, when aerosols are likely influenced significantly by emissions from biomass burning, coal burning etc. ~~Moreover, none of the previous AMS measurements studied the aerosol characteristics during springtime in Nanjing.~~ For these reasons, we reports in this work, ~~for the first time,~~ the real-time measurement results on urban fine aerosols in Nanjing using the SP-AMS during spring in 2015. The rich highly-time resolved, highly-chemical resolved ~~lution~~ mass spectral ~~(HRMS)~~ data, as well as chemically-resolved size distributions of different aerosol species obtained for the first time in Nanjing during this study, can allow us to conduct in-depth analyses, and better understand the characteristics, sources and relevant transformation processes of ambient aerosols in Nanjing. The findings for such a megacity are also valuable to the Pan-Eurasian Experiment (PEEX) infrastructure which aims to resolve the major uncertainties in Earth system science and global sustainability issues (Kulmala et al., 2015).~~.~~

2. Experiments

2.1 Sampling site and instrumentation

The field campaign was conducted in the environment monitoring station of Nanjing Olympic center (32°0′33.00″N, 118°44′9.53″E, Fig. S1) from April 13 to 29,

2015. Details of the sampling site are shown in Fig. S1. The site was surrounded by residential buildings, close to a few urban arterial roads (~ 85 m northwest of Huangshan Road, ~ 200 m northeast to Mengdu Street and ~425 m southwest of Xinglong Street). There are also a restaurant (~50 m), a student cafeteria (~300 m), and the Nanjing Cigarette Factory (~480 m southeast) around the site.

The sampling inlet was installed outside the fifth floor of the building (~12 m above the ground), with a $PM_{2.5}$ cyclone (URG Corp., Chapel Hill, NC, USA) to remove coarse particles. Ambient particles were dried (RH <10%) via a diffusion dryer filled with silica gel before entering into the SP-AMS. The sampling line (~2 m long) was assembled using stainless steel tubing and proper fittings. Air flow was controlled at around ~5 L min^{-1}, with a flow rate into the SP-AMS at ~80 cm^3 min^{-1}.

The SP-AMS can measure non-refractory (NR) PM_1 components including ammonium, nitrate, sulfate, chloride and organics similar to other types of AMS via a thermal tungsten heater. Moreover, it can also measure *r*BC and inorganic/organic ~~and coated~~ species that coated on the *r*BC cores, as it is equipped with an intracavity Nd:YAG laser vaporizer (1064 nm) (Onasch et al., 2012). During this campaign, the instrument was switched between "laser on" and "laser off" settings, and between V-mode (better for mass quantification) and W-mode (better chemical resolution, ~5000 in this study), with one cycle including six menu settings (M1: Laser on V-mode; M2: Laser off V-mode; M3: Laser on W-mode; M4: Laser off W-mode; M7: Laser on PToF-mode; M8: Laser off PToF-mode). Each menu was set to 2.5 min, thus a full running cycle lasted for 15 mins. The PToF-mode was under V-mode, but was tuned in particular for measuring particle sizes. The tungsten heater was always turned on and kept at ~600^{o}C.

The SP-AMS, in conjunction with a scanning mobility particle sizer (SMPS) (TSI inc., Shoreview, MN, USA) was calibrated for mass quantification (e.g., ionization efficiency) using size-selected (250 nm and 300 nm) monodisperse ammonium nitrate particles following the procedures detailed in Jimenez et al. (2003). Pure ammonium sulfate was used to determine the relative ionization efficiency (RIE) of sulfate

(Setyan et al., 2012). Quantification of *r*BC was calibrated using Regal Black (REGAL 400R pigment black, Cabot Corp.) particles according to the procedures reported in Onasch et al. (2012). Note that the solution of Regal Black was sonicated during calibration to maintain a relative stable aerosol flow. RIEs of ammonium, nitrate, sulfate, chloride, organics and *r*BC were determined to be 3.15, 1.05, 1.20, 1.3, 1.4 and 0.33, respectively. On the other hand, particle sizing was calibrated using standard polystyrene latex (PSL) spheres (Duke Scientific Corp., Palo Alto, CA, USA) across 100 - 700 nm range. Flow rate was also calibrated prior to the measurement.

Concentrations of gaseous species, e.g., carbon monoxide (CO) (Model T300, Teledyne API, USA), ozone (O_3) (Model EC9810, Ecotech Pty Ltd, Australia), nitrogen dioxide (NO_2) and sulfur dioxide (SO_2) (Model LGH-01, Anhui Landun, China), and meteorological data including air temperature (T), relative humidity (RH), visibility (km), wind speed (WS) and wind direction (WD) were acquired at the same site. $PM_{2.5}$ and PM_{10} mass concentrations were also recorded (BAM-1020, Met One Instruments, Inc., USA), in parallel with the SP-AMS measurement.

2.2 Data treatment and source analyses

The SP-AMS data were post-processed by using the Igor-based standard ToF-AMS Analysis Toolkit SQUIRREL v1.56D and PIKA v1.15D, available at: http://cires1.colorado.edu/jimenez-group/ToFAMSResources/ToFSoftware/index.html. Note all mass concentrations reported here were calculated from the HR fitted results on V-mode data. A collection efficiency is typically used to account for the particles that aren't collected and measured by the instrument, due to the particles lost during passage through inlet, time-of-flight chamber and bouncing from the vaporizer. For the SP-AMS, the CE of laser vaporizer is mainly governed by particle divergence, while for the tungsten vaporizer, the CE is governed mainly by the bouncing effects (Matthew et al., 2008). A CE value of 0.5 is valid and used commonly for the AMS measurements for most environments (Canagaratna et al., 2007). Nevertheless, Middlebrook et al. (2012) further investigated this issue, and found that high aerosol acidity, high ammonium nitrate, and high sampling line RH can increase the CE, and

域代码已更改

provide composition-dependent CE parametrization. For our dataset, we found that the composition-dependent CE rather than a constant CE=0.5 has negligible effects on the quantification of aerosol species, as the particles were neutralized (Fig. 3a), the mass fraction of ammonium nitrate were <40% in almost all cases, and also the sampling line RH was below 10%. And in fact, the PM_1 mass concentrations quantified by using the composition-dependent CE correlate a bit worse with the $PM_{2.5}$ concentrations than ones using CE=0.5. Thus, we a constant CE of 0.5, in consistent with many other AMS studies, was employed for this dataset.~~A constant collection efficiency (CE) of 0.5 was used for the mass quantification, in consistent with many other AMS studies, as indeed the mass fraction of ammonium nitrate (mostly <40%), particle acidity (near neutral) and RH (<10%) do not affect the CE significantly for this dataset (Middlebrook et al., 2012).~~

Unless specified, the concentrations of ammonium, sulfate, nitrate, chloride and organics are from M2 setting (tungsten vaporizer only), while the *r*BC data is from M1 setting (dual-vaporizers: tungsten + laser) in this paper. The meteorological data (RH, T, WS, WD and visibility), concentrations of gas-phase species (CO, NO_2, SO_2 and O_3) and $PM_{2.5}$ were averaged into hourly data for comparisons with the SP-AMS data. The data reported are at local time, e.g., Beijing (BJ) Time.

Positive matrix factorization (PMF) (Paatero and Tapper, 1994) was applied on the high resolution mass spectra (HRMS)~~HRMS~~ of organic aerosol (OA) obtained under laser off W-mode (M4 setting) to elucidate the OA sources/processes. We used the PMF Evaluation Tool version 2.08A (downloaded from: http://cires1.colorado.edu/jimenez-group/wiki/index.php/PMF-AMS_Analysis_Guide) (Ulbrich et al., 2009) to investigate the PMF results by varying the number of factors (from 2 to 8 factors) and rotations ("*f*peak", from -1 to 1 with an increment of 0.1). Only ions with *m/z* less than or equal to 180 were included in the analyses. Following the instruction detailed by Zhang et al. (2011), the 4-factor solution (at *f*peak = -0.1) was chosen as the optimal solution, as the 3-factor solution cannot separate the hydrocarbon-like OA (HOA) and cooking OA (COA) (Fig. S2). For the 5-factor

solution (Fig. S3), Factor 2 and Factor 4 are clearly a split from the SVOOA from the 4-factor solution (r^2 = 0.89 and slope of 1.05); Factor 2 of 5-factor solution also shows much weaker correlations with nitrate than SVOOA of 4-factor solution does (r = 0.07 vs. 0.49). ~~, and the 5-factor solution clearly splits the semi-volatile oxygenated OA (SV-OOA) factor into two OOA factors (Fig. S3).~~ A summary of the key diagnostic plots are provided in Fig. S4. Detailed discussion of the PMF results is presented in Section 3.5. Note we found no significant differences between the PMF source apportionment results from the HRMS of OA (without *r*BC) obtained with dual-vaporizers setting (M3 setting) and current results (M4 setting, tungsten vaporizer only), as the OA HRMS acquired under these two circumstances were overall very similar (details in Section 3.4).

Note the elemental ratios shown throughout the paper were all calculated based on the method proposed by Aiken et al. (2008) (referred to as A-A method). Recently, Canagaratna et al. (2015) improved this methodology by using specific ion fragments as markers to calculate the O/C and H/C ratios (referred to as I-A method). The I-A method increased the O/C ratio, H/C ratio, and the OM/OC ratio from the values calculated from the A-A method, on average, by 28%, 10% and 8%, respectively (Fig. S5). In this work, we used the results from the A-A method for consistency and comparisons with previous AMS measurements.

3. Results and discussion

3.1 Mass concentrations, chemical compositions and diurnal changes

The temporal variations of meteorological parameters, concentrations of the gas pollutants, concentrations and mass fractions of different PM_1 components, and the $PM_{2.5}$ mass loadings (from Met one BAM-1020) over the sampling period are illustrated in Fig. 1. During this study, the mean temperature was 18.5 ^oC, RH on average was 64%, and wind predominantly blew from southeast and southwest (Fig. S6~~5~~). The SP-AMS PM_1 concentrations ranged from 5.1 to 97.9 μg m^{-3}, with an

average of 28.2 μg m^{-3}. Note this average PM_1 concentration is significantly lower than those observed during summer (38.5 μg m^{-3}), autumn (46.4 μg m^{-3}) and winter (89.3 μg m^{-3}) (Zhang et al., 2015;Zhang et al., 2016b), showing that the air during springtime in Nanjing is cleaner than in other seasons. The variations of PM_1 concentrations also match very well with $PM_{2.5}$ concentrations (Pearson's $r^2 = 0.72$), and on average PM_1 accounts for ~ 54% of the $PM_{2.5}$ mass. This ratio appears to be a bit low, likely due to the uncertainty of CE of the SP-AMS.

The average PM_1 composition is shown in Fig. 2a. The most abundant component is found to be organics (45.0%), following by sulfate (19.3%), nitrate (13.6%), ammonium (11.1%), *r*BC (9.7%) and chloride (1.3%). Fig. 2b further shows changes of the PM_1 chemical compositions in different concentration bins. It can be seen that although most PM_1 mass loadings are within 10 - 40 μg m^{-3}, high loading periods tend to have higher mass contributions from organics and *r*BC, and less contributions from secondary inorganic species, indicating that high PM events were influenced significantly by local fresh emissions.

The molar ratio of inorganic anions (sulfate, nitrate and chloride) to cations (ammonium) is 1.05 (Fig. 3a) (Zhang et al., 2007b). Considering that a small fraction of sulfate, nitrate and chloride are possibly associated with metal cations, such as Na^+, K^+ and Ca^{2+}, etc.，it can be concluded that the NR-PM_1 was overall neutral throughout the study. On the other hand, the molar ratio of inorganic anions to ammonium is on average 1.17 (Fig. 3b) when dual-vaporizers are on. This may be partially due to variations of ionization/collection efficiencies of the measured species as the addition of laser beam may change the distribution of vaporized species inside the ion chamber, and also because of the detection of sulfate, nitrate and chloride bonded with metal cations under the dual-vaporizers. These species don't evaporate on the tungsten vaporizer under the laser-off mode. Indeed, more metal signals were observed with the dual-vaporizers, as shown in Fig. ~~S6~~S7.

Fig. 2c shows the average diurnal changes of organics, sulfate, nitrate, chloride and *r*BC. Sulfate concentrations are slightly higher during daytime than during

nighttime, indicating a significant contribution from photochemical reactions. Sulfate also shows the least variations among all species, reflecting its regional behavior. Except for sulfate, all other species present a dual-peak pattern, with one peak in early morning and another one in early evening. The peaks of *r*BC and organics are likely due to local traffic/cooking activities (see details in Section 3.5), while the behavior of nitrate is likely driven by the thermodynamic gas-particle partitioning: $NH_3(g) + HNO_3(g) \leftrightarrow NH_4NO_3(p)$ ~~$\leftrightarrow NH_3(g) + HNO_3(g)$,~~ as it shows good anti-correlations with the diurnal changes of temperatures (r = -0.72 for nitrate *vs.* T). The good correlations between the diurnal cycles of nitrate and RH, in particular during nighttime, suggest a nighttime formation pathway of nitrate, e.g., $N_2O_5 + H_2O = 2HNO_3$ and $HNO_3 + NH_3 = NH_4NO_3$. Furthermore, we calculated the diurnal variations of the equilibrium constant of NH_4NO_3 ($K_{p,AN}$) (Seinfeld and Pandis, 2006;Young et al., 2016) in Fig. 2c. The $K_{p,AN}$ displays a similar trend as nitrate (r = 0.68), providing strong evidence that nitrate variations were governed mainly by the thermodynamic equilibrium. Chloride shows similar behavior as nitrate, indicating it is driven by the equilibrium $NH_3(g) + HCl(g) \leftrightarrow NH_4Cl(p)$ ~~$\leftrightarrow NH_3(g) + HCl(g)$,~~ as well ($r$ = -0.76 for chloride *vs.* T). Therefore, when temperature rises, more NH_4NO_3 and NH_4Cl can dissociate into gaseous NH_3, HNO_3 and HCl, mass loadings of particle-phase nitrate and chloride decrease correspondingly, and *vice versa*.

In order to further elucidate the formation processes of ~~of nitrate and~~ sulfate, we calculated the oxidation ratios of sulfur (f_S) ~~and nitrogen (f_N)~~ (Fig. 4a ~~and 4b~~), defined as $f_S = nSO_4^{2-}/(nSO_4^{2-} + nSO_2)$ ~~and $f_N = nNO_3^-/(nNO_3^- + nNO_2)$~~ (Xu et al., 2014), indicating the conversion of SO_2 ~~and NO_2 to sulfate and nitrate, respectively~~. Here nSO_4^{2-} and ~~, nNO_3^- ,~~ nSO_2 ~~and nNO_2~~ are the molar quantities of particle-phase sulfate, and ~~sulfate and nitrate,~~ gas-phase SO_2 ~~and NO_2~~, respectively. Diurnal variations of f_S and RH ~~, f_N and mass ratios of SO_4^{2-}/NO_3^-~~ are presented in Fig. ~~4b, and Fig. 4c~~ shows variations of sulfate and nitrate concentrations with RH ~~4d-f, along with the diurnal cycle of RH~~. The diurnal profile of f_S shows a negative correlation with that of RH (r = - 0.52), and mass concentrations of sulfate even drop under high RH conditions,

indicating an insignificant role of aqueous-phase processing for sulfate formation during this campaign. On the other hand, t~~T~~he f_S reaches a maximum around 3 pm. Note the afternoon rise of fs and sulfate may be affected by the down mixing of sulfate formed earlier, however, since concentrations of all other aerosol species that mix with sulfate decrease significantly, we postulate that the increase of *f*s likely suggest the photochemical production of sulfate in the afternoon. ~~; similarly, the SO_4^{2-}/NO_3^- ratios are elevated significantly during daytime, in particular during afternoon. These behaviors suggest the remarkable role of photochemical processing of SO_2 to sulfate. In addition, the diurnal profile of f_S shows a negative correlation with that of RH (r = -0.52), indicating somewhat insignificant influence of aqueous phase production of sulfate during this campaign. Interestingly, during nighttime (7 pm – 6 am), variations of f_N follows the changes of RH, probably suggesting a nighttime formation pathway of nitrate, e.g., $N_2O_5 + H_2O = 2HNO_3$ and $HNO_3 + NH_3 = NH_4NO_3$; while the afternoon drop of f_N is likely due to evaporation of nitrate as the temperature increases.~~

3.2 Chemically-resolved size distributions

The campaign-averaged mass-based size distributions, fractional contributions and diurnal size distributions (image plots) of the major PM_1 species are depicted in Fig. 5 (temporal variations of the mass-based size distributions of these PM_1 species over the whole measurement period are provided in Fig. ~~S7~~S8). Note the size distribution of *r*BC in these plots were scaled from the size distribution of *m/z* 24 (C_2^+), as other major *r*BC ion clusters may be heavily influenced by other ions, such as C^+ signal but from organics at *m/z* 12 (C^+), HCl^+ signal at *m/z* 36 (C_3^+), SO^+ signal at *m/z* 48 (C_4^+), $C_2H_4O_2^+$ signal at *m/z* 60 (C_5^+). It also should be note that, although the AMS is able to capture the bulk of atmospheric accumulation mode particles (Canagaratna et al., 2007), right side of size distributions may be affected by the incomplete transmission of larger particles limited by the SP-AMS inlet (in particular, the supermicron ones).

As can be expected, all inorganic species (sulfate, nitrate, chloride and ammonium) display a unimodal distribution with an accumulation mode peaking ~550 nm (vacuum aerodynamic diameter, D_{va} (DeCarlo et al., 2004)), since they were mainly formed from secondary reactions. The organics has a much broader size distribution across from ultrafine (<100 nm) to supermicron meter range, with a small sub-peak centering ~120 nm in addition to the major peak at ~440 nm, indicating influences from both primary and secondary emissions. On the contrary, size distribution of *r*BC behaves very differently from other components, which peaks at 90 - 200 nm range, reflecting clearly that it is mainly originated from primary emissions. Overall, the small particles are predominantly consisted of organics and *r*BC, which together account for more than 90% of the ultrafine particle mass. Mass contributions from inorganic species increase significantly with the increase of particle size, and they dominate masses of particles larger than 400 nm (Fig. 5b).

In line with the diurnal mass loadings of the PM_1 species shown in Fig. 2c, the diurnal size distribution of sulfate is generally stable, with masses concentrating in the 400 - 700 nm range throughout the day (Fig. 5c); while the size distributions of nitrate, chloride and organics present clear enhancements in the 300 - 700 nm range during early morning and early evening due to increased mass concentrations of these species during these two periods. The size distribution of *r*BC is also enhanced during the morning and evening hours, but it extends to a much smaller size range (<100 nm).

3.3 PM_1 contributions on visibility impairment

In order to figure out the major species that are responsible for the visibility degradation, here we employed the IMPROVE method to reconstruct the light extinction coefficients (b_{ext}). b_{ext} values are derived from the measured visibility: $b_{ext}=3.91/V_s$ (Kong et al., 2015), where V_s stands for the visibility (in meter). The following IMPROVE formula (Yang et al., 2007) was used:

$$b_{ext} = 3f(RH)\{[(NH_4)_2SO_4] + [NH_4NO_3] + [NH_4Cl]\} + 4[OM] + 10[BC] + 1[soil]+10$$

Where f(RH) is a RH-dependent empirical coefficient which considers the effects of

water uptake by inorganic salts on the light extinction; the *f*(RH) values used here were taken from Malm and Day (2001), which were regressed from the Great Smoky data set. [$(NH_4)_2SO_4$], [NH_4NO_3], [NH_4Cl], [OM], and [BC] represent the mass concentrations of ammonium sulfate, ammonium nitrate, ammonium chloride, organics and black carbon directly from the SP-AMS measurements (in μg m^{-3}) ([$(NH_4)_2SO_4$] = 1.375*[SO_4^{2-}], [NH_4NO_3]=1.29*[NO_3^-] and [NH_4Cl] = 1.51*[Cl^-]). Since the SP-AMS cannot accurately measure soil components (e.g., various metals/metal oxides/metal salts), the term [soil] was set to zero during calculations.

By using this method, the reconstructed visibilities match reasonably well with the measured values (r^2 = 0.50) as shown in Fig. 6a. Fig. 6b shows the time series of the measured and reconstructed extinction coefficients throughout the whole sampling period. It should be noted that, on average, the measured PM_1 species are only able to explain ~44% of the light extinction. This is likely due to that: 1) as shown earlier, the SP-AMS measured PM_1 only occupies ~54% of the $PM_{2.5}$ mass; 2) we didn't include contributions from soil components, coarse particles and also some gas-phase species (such as NO_2); 3) although the influences of water are included in part through *f*(RH) for inorganic salts, the water uptake by organic species are not considered explicitly, which can be significant especially for the SOA under high RH conditions (Duplissy et al., 2011;Denjean et al., 2015). Indeed, as shown in Fig. 6a, reconstructed visibilities appear to deviate more significantly from the measured visibilities under high RH than ones under low RH conditions, suggesting the importance of particle-bounded water on visibility degradation. The pie chart in Fig. 6b presents the average relative contributions of different components to the light extinction of PM_1. The largest contributor is organics which accounts for 37.7%, followed by ammonium sulfate (25.1%), *r*BC (20.7%), ammonium nitrate (15.1%) and a minor contributor of ammonium chloride (1.4%).

3.4 Chemical characteristics of OA

The unique laser vaporizer of SP-AMS allows it to detect *r*BC and species coated

406 on the *r*BC core including both non-refractory and refractory organics, thus
407 comparison between the OA mass spectra obtained with dual-vaporizers and tungsten
408 vaporizer settings, can infer some information regarding the chemical features of
409 refractory organics, which ~~that~~ were unable to be determined by any other types of
410 AMS. As shown in Fig. 7a and 7b, the OA obtained with dual-vaporizers setting have
411 slightly higher oxygen-to-carbon (O/C) ratio (0.28 *vs.* 0.27), nitrogen-to-carbon (N/C)
412 ratio (0.033 *vs.* 0.032) and lower hydrogen-to-carbon (H/C) ratio (1.50 *vs.* 1.52) than
413 the corresponding elemental ratios of OA obtained with the tungsten vaporizer only.
414 This result indicates that refractory organics are likely more oxygenated than the
415 non-refractory organics, and for this dataset it is mainly due to a higher fractional
416 contribution from $C_2H_3O^+$ (see the inset of Fig. 7a). This is different from the results
417 on laboratory-generated nascent soot, where larger fCO_2^+ (i.e., the fraction of total
418 organic signal contributed by CO_2^+) was observed with the dual-vaporizers setting,
419 indicating the variability of the chemical compositions of refractory organics.
420 ~~Note the elemental ratios shown throughout the paper were all calculated based~~
421 ~~on the method proposed by Aiken et al. (2008) (referred to as A-A method). Recently,~~
422 ~~Canagaratna et al. (2015) improved this methodology by using specific ion fragments~~
423 ~~as markers to calculate the O/C and H/C ratios (referred to as I-A method). The I-A~~
424 ~~method increased the O/C ratio, H/C ratio, and the OM/OC ratio higher than the~~
425 ~~values calculated from the the A-A method, on average, by 28%, 10% and 8%,~~
426 ~~respectively (Fig. S8). In this work, we used the results from the A-A method for~~
427 ~~consistency and comparisons with previous AMS measurements.~~ It should be noted
428 that, accurate determination of refractory organics is very difficult, because: 1) A large
429 portion of refractory organics cannot be detected by the SP-AMS if they didn't coat on
430 *r*BC cores; 2) To accurately measure the species only coated on *r*BC cores, the
431 tungsten vaporizer has to be physically removed, otherwise the vaporizer temperature
432 is still around 150°C even its power is turned off, and the non-refractory organics that
433 don't coat on *r*BC cores can still be measured, and complicates the analyses; 3) The
434 CE and IE values for different species may vary under different vaporizer settings, so

域代码已更改

域代码已更改

that direct subtraction of organics measured under tungsten-only setting from the organics measured under dual-vaporizer setting may not represent the real refractory organics; 4) Some ions measured under dual-vaporizer setting are likely induced by the laser itself rather than the 70 ev electron impact. For example, a series of fullerene-like carbon clusters can be generated by the laser itself, even though they don't really exist in the atmosphere (Wang et al., 2016a;Onasch et al., 2015). This laser-induced ion formation scheme may work for other organics, thus makes it even more difficult for identifying the refractory organics. Further studies are essential to investigate this issue. –

域代码已更改

Overall, the O/C ratio (0.27) of OA in Nanjing during springtime is a bit lower than those observed at other urban locations in China – for instances, 0.30 in Shenzhen (He et al., 2011), 0.31 in Shanghai (Huang et al., 2012b), 0.33 in Lanzhou (Xu et al., 2014) and 0.34 in Beijing (Zhang et al., 2014), and much lower than those at rural sites – for instances, 0.47 in Kaiping (Huang et al., 2011) and 0.59 in Changdao (Hu et al., 2013). As O/C ratio is a good indicator of the aging degree of OA, the relatively low O/C level indicates a significant contribution from fresh emissions in Nanjing aerosols during springtime. Accordingly, the non-refractory OA (pie chart in Fig. 7b) is dominated in hydrocarbon $C_xH_y^+$ ions (51.2%) rather than the oxygen-containing ion fragments (37.4% of $C_xH_yO_1^+$ and $C_xH_yO_2^+$).

The scatter plot of *f*44 (mass fraction of *m/z* 44 to the total OA) *vs.* *f*43 (mass fraction of *m/z* 43 to the total OA) (a.k.a., triangle plot) (Ng et al., 2010) was often used to investigate the oxidation degrees of OA. As presented in Fig. 8, most OA reside in the bottom end of the triangular region, again pointing out the less-oxygenated behavior of the OA. Since the HRMS can separate different ions at the nominal *m/z*, we also examined the fCO_2^+ *vs.* $fC_2H_3O^+$ space and illustrated it in Fig. S9 - many OA locate outside the triangular region, yet still close to the bottom. Moreover, *m/z* 60 (mainly $C_2H_4O_2^+$) is a significant fragment ion of levoglucosan, which is well known as the biomass burning aerosol tracer (Alfarra et al., 2007). However, as *f*60 (mass fraction of *m/z* 60 to the total OA) is very low in OA (average

464 ± 1σ = 0.4 ± 0.06 %), indicating no biomass burning influences on the OA properties
465 during springtime in Nanjing.
466
467 **3.5 Sources and evolution processes of OA**
468 In order to further elucidate the sources and evolution processes of OA, we
469 performed PMF analyses and identified four OA components, including two primary
470 OA (POA) factors – a traffic-related hydrocarbon-like OA (HOA) and a
471 cooking-related OA (COA), and two secondary OA factors – a semi-volatile
472 oxygenated OA (SV-OOA) and a low volatility OOA (LV-OOA). Details about their
473 characteristics are discussed below.
474 **3.5.1 Mass spectral features of the OA factors**
475 The mass spectral profiles, time-dependent mass concentrations of the four OA
476 factors and corresponding tracer ions are presented in Fig. 9. The HOA mass spectrum
477 is overall dominated by the $C_xH_y^+$ ions (73.2%), such as $C_3H_7^+$, $C_4H_7^+$, $C_4H_9^+$, $C_5H_9^+$
478 etc., which are most likely produced from alkanes and cycloalkanes emitted from fuel
479 and lubricating oil burning (Canagaratna et al., 2004). This feature is in good
480 agreement with the mass spectral features of POA directly from vehicle
481 emissions(Collier et al., 2015), and the HOA factors determined in many other
482 locations (e.g., Ge et al., 2012b;Huang et al., 2010;Sun et al., 2011). HOA has the
483 lowest O/C ratio (0.10) and highest H/C ratio (1.75) among all factors, representing its
484 behavior as primary fresh emissions. The COA mass spectrum is also rich in $C_xH_y^+$
485 ions (64.7%), but having more oxygenated ions ($C_xH_yO_z^+$) than the HOA (26.5% *vs.*
486 15.4%), especially $C_3H_3O^+$ and $C_3H_5O^+$ ions. The significant contributions of $C_3H_3O^+$
487 and $C_3H_5O^+$ to *m/z* 55 and *m/z* 57 are a common feature of COA, that has been
488 reported in various urban locations around the world, for examples, Beijing (Sun et al.,
489 2015a), London (Allan et al., 2010), Fresno (Ge et al., 2012b), New York City (Sun et
490 al., 2011) and Barcelona (Mohr et al., 2012;Mohr et al., 2015). These
491 oxygen-containing ions are in part generated from the fragmentation of fatty acids in
492 the cooking aerosols (Ge et al., 2012b). As a result, COA has a higher O/C ratio of

493 0.16 and a lower H/C ratio of 1.67 than those of HOA. The O/C and H/C levels of
494 COA in this work are also close to those identified in other locations aforementioned.
495 The consistency of the chemical characteristics of COA from such different locations
496 suggests that ambient COA is more relevant to the cooking oil rather than the different
497 types of food, which was postulated earlier by Allan et al. (2010).

498 Unlike the two POA factors, SV-OOA and LV-OOA are both abundant in
499 oxygen-containing fragments ($C_xH_yO_z^+$ ions), which are 46.4% and 54.8%,
500 respectively. The higher O/C ratio (0.55 *vs.* 0.32) and more $C_xH_yO_2^+$ ions (18.8% *vs.*
501 11.8%) in the LV-OOA mass spectrum than those of the SV-OOA, reflecting the fact
502 that LV-OOA went through more aging/oxidation reactions than ~~the~~ SV-OOA. The
503 O/C ratio of SV-OOA is 0.32, which is within the O/C range of SV-OOA observed
504 worldwide (Jimenez et al., 2009). The LV-OOA O/C ratio of 0.55 is in the lower end
505 compared to the O/C levels of LV-OOA observed in other China sites, for examples,
506 0.64 in Kaiping (Huang et al., 2011), 0.65 in Shanghai (Huang et al., 2012b), 0.68 in
507 Lanzhou (Xu et al., 2014), 0.78 in Changdao (Hu et al., 2013) and 0.80 in Hong Kong
508 (Lee et al., 2013).

509 Consistently, in the *f*44 *vs.* *f*43 space (Fig. 8), SV-OOA situates near the bottom
510 side while LV-OOA approaches to the upper part of the triangular region, because of a
511 much larger fractional contribution of CO_2^+ in the LV-OOA mass spectrum. HOA and
512 COA, as POA factors, both reside in the bottom end of the plot, away from SV-OOA
513 and LV-OOA; while they locate outside the triangle in the fCO_2^+ *vs.* $fC_2H_3O^+$ space
514 (Fig. S9), indicating that the HRMS acquired by the SP-AMS is better in
515 differentiating POA factors from other SOA factors than the unit mass resolution
516 (UMR) data.

517 In order to justify the OA factors identified in this study, we compared the
518 spectral similarities of the OA factor spectral profiles (in both HR and UMR) with
519 those separated during wintertime in Beijing (Sun et al., 2015a), summertime in
520 Lanzhou (Xu et al., 2014), and wintertime in Fresno (Ge et al., 2012b;Ge et al.,
521 2012a). The results are listed in Table 1. Indeed, the HOA, COA and LV-OOA mass

spectra are highly similar to the corresponding factors identified in Bejing, Lanzhou and Fresno (r^2 > 0.87); SV-OOA also correlates fairly well with Bejing and Lanzhou SV-OOA too, but with relative low r^2 (0.68 – 0.75), mainly because of one or two ion fragments, namely, higher CO^+ and CO_2^+ signals in Beijing SV-OOA and higher $C_2H_3O^+$ signal in Lanzhou SV-OOA than those in Nanjing SV-OOA. The SV-OOA on the other hand, correlates very well with the Fresno OOA (r^2 = 0.90 and 0.91).

Moreover, as presented in Fig. 9a, the HOA mass spectrum contains relatively higher fraction of ions with large *m/z* values (*m/z* > 100) than that of COA (14.0% *vs.* 8.2%), and most of these ions are $C_xH_y^+$ ions, probably from fuel burning emitted long-chain alkanes, etc. The SV-OOA also includes more large *m/z* ion fragments (*m/z*> 100) than those in the LV-OOA mass spectrum (10.5% *vs.* 5.3%), likely suggesting that further oxidation of SOA species may lead to the fragmentation of high molecular weight species and formation of small molecules – a mechanism verified by both lab-scale experiments (e.g., Yu et al., 2014) and field measurements (e.g., Lee et al., 2012).

3.5.2 Temporal variations, diurnal patterns and relative contributions of the OA factors

The temporal variations of different OA factors and their corresponding tracer ions are displayed in Fig. 9b. $C_4H_9^+$ ion, a.k.a., the HOA mass spectral tracer (Zhang et al., 2005) indeed varies very closely to the HOA (r^2= 0.94). Time series of the COA tracer ion $C_6H_{10}O^+$ (and also $C_5H_8O^+$, $C_7H_{12}O^+$) (Sun et al., 2011;Ge et al., 2012b) match very well with that of COA too (r^2 = 0.90). SV-OOA correlates better with $C_2H_3O^+$ (r^2 = 0.90) than with CO_2^+ (r^2 = 0.66). Although LV-OOA doesn't correlate very well with CO_2^+ (r^2 = 0.12) mainly due to the mismatch during April 23 - 26, the correlation is still much better than it with $C_2H_3O^+$ (r^2 < 0.001). In Table 2, we tabulate the correlation coefficients (*r*) of the four OA factors with the gas-phase species, BC and inorganic species. Note we used Pearson's *r* not r^2 here since some correlation coefficients are negative. From the table, it is clear that the traffic-related gaseous species, CO and NO_2, correlate best with HOA among all OA factors;

SV-OOA correlates better with nitrate (r = 0.49) than it with sulfate (r = 0.11); LV-OOA correlate better with sulfate (r = 0.23) that it with nitrate (r = 0.11). All these results are consistent with the traffic origin of HOA, the semi-volatile and low-volatility behaviors of SV-OOA and LV-OOA.

Accordingly, diurnal cycles of the OA factors are presented in Fig. 10a. Correlation coefficients (r) of the diurnal variations between OA factors with gas-phases and inorganic species are provided in Table 2, as well. HOA concentrations show an early morning peak, and it overall remains at high levels during nighttime. Besides the impacts of boundary layer height, this is also due to enhanced emissions from construction vehicles around the site, which were in fact much more active during nighttime than during daytime because of the restrictions of Nanjing government. Most of those vehicles used low-quality diesel fuel, and could emit a large amount of *r*BC particles. The *r*BC diurnal pattern is indeed almost identical to that of HOA (r =0.99), indicating that the HOA during this campaign was apparently associated with the construction vehicle emissions. COA concentrations increase during noon (12 pm – 1 pm) and early evening, in response to the lunchtime and dinnertime cooking activities. SV-OOA concentrations decreases from 9 am, and reach a minimum during afternoon (3 pm – 4 pm), oppositely to the variation of temperatures (r = -0.85) but similar to that of nitrate (r = 0.53), corroborating its semi-volatile feature. Different from other factors, LV-OOA concentrations increase during daytime and shows positive correlation with temperature (r = 0.76); it also has negative correlation with the diurnal cycle of RH (r = -0.75). Both behaviors are similar to those of sulfate (r = 0.72 for the diurnal cycle of LV-OOA *vs.* sulfate), indicating the leading role of photochemical oxidation for LV-OOA formation as well.

As shown in Fig. 10b, due to mainly the increase of LV-OOA mass loading, OA is overwhelmingly dominated by the SOA (SV-OOA + LV-OOA) during afternoon (80.2% at 3 pm); POA (HOA + COA) only dominates the OA mass during morning (53.2% at 7 am) and early evening (56.9% at 8 pm) in response to the enhanced traffic and cooking emissions. On average, the OA is composed of 27.6% of HOA, 16.9% of

COA, 27.4% of SV-OOA and 28.1% of LV-OOA (Fig. 10c), with SOA outweighing POA (55.5% *vs.* 44.5%). However, as shown in Fig. 10d, with the increase of OA mass loadings, the fractional contribution of POA increases, highlighting the important and direct influences of anthropogenic emissions on the heavy pollution haze events.

3.5.3 Local/regional influences and evolution processes of the OA factors

Combining WS, WD and mass loadings, the bivariate polar plots of the four OA factors, *r*BC, ~~and~~ total OA, nitrate, sulfate and the total PM_{1}~~+~~ are shown in Fig. 11. These plots provide an effective graphical method for showing the potential influences of air masses from different directions with different wind speeds to the receptor site (Carslaw and Beevers, 2013). Clearly, high mass loadings of HOA and *r*BC mostly link with low WS (< 1 m s^{-1}), indicating they are mainly from local vehicle emissions. High COA concentrations occur mainly under low WS as well, but with some high concentrations accompanied with air masses from southeast under higher WS. SV-OOA appears to be mainly formed locally, except for a concentration hotspot in the southeast – likely due to emissions from the tobacco factory that resides in that direction. Nitrate, as a semi-volatile species, behaves overall similar to the SV-OOA. High concentrations of LV-OOA are distributed in all directions under higher WS, similar to that of sulfate, representing their~~its~~ regional behaviors. Overall, high PM_1 mass loadings occur mainly under low WS, indicating that the PM_1 is heavily affected by local emissions rather than pollutants in a regional scale.

The aging of OA can be described in general by the increase of O/C and decrease of H/C. In this regard, we plotted the Van Krevelen diagram (Heald et al., 2010) (Fig. 12a) to show the relationships between H/C and O/C ratios for all OA as well as the four OA factors. Overall, in this study, the H/C and O/C ratios of OA data are correlated linearly with a slope of -1.04 (r^2 = 0.93). ~~, indicating the propagation of OA is similar to an aging process that is likely driven by the addition of carboxylic acid (slope of -1).~~ Interestingly, the two OOA factors lie very well on the fitted straight line.

609 This trend may suggest that the evolution of secondary OA during this campaign
610 follows a transformation pathway of SV-OOA to LV-OOA ~~through the addition of~~
611 ~~carboxylic acid~~. The diurnal cycle of LV-OOA varies oppositely to that of SV-OOA (r
612 = -0.86), probably supporting this hypothesis. In addition, SV-OOA and LV-OOA
613 mass concentrations, and O/C ratios of OA all show no obvious correlations with the
614 RH as shown in Fig. 12b and Fig. 12c, indicating~~verifying~~ that aqueous-phase
615 processing is insignificant compared to the photochemical processing for the
616 oxidation of OA.
617
618 **4. Conclusions**
619 We present for the first time the real-time measurement results using the SP-AMS
620 on submicron aerosols in urban Nanjing during springtime (April 13 - 29, 2015). The
621 dynamic variations of SP-AMS determined PM_1 mass loadings, agreed well with the
622 $PM_{2.5}$ ~~concentrations~~ measured by the Met One $PM_{2.5}$ analyzer. The average PM_1
623 concentration was 28.2 μg m^{-3}, lower than previously ACSM-determined PM_1
624 concentrations during summer and winter in Nanjing. Organics on average comprised
625 the largest fraction (45%) of PM_1, and its fractional contributions increased in case of
626 high PM_1 mass loadings. The diurnal cycles of mass concentrations of organics, rBC,
627 nitrate and chloride all presented a similar behavior, which was high in early morning
628 and evening, but low in the afternoon. Concentrations of sulfate, on the contrary,
629 increased during afternoon. Further investigations of f_S, sulfate concentrations and its
630 relationship with ~~, f_N, SO_4^{2-}/NO_3, and~~ RH ~~revealed~~ suggest that photochemical
631 processing contributed significantly to sulfate formation compared to the
632 aqueous-phase processing, while nitrate (and chloride) formation was mainly
633 governed by the thermodynamic equilibrium. The chemically-resolved mass-based
634 size distribution data showed that rBC occupied a large fraction of ultrafine particles,
635 while secondary inorganic species could dominate the mass of particles larger than
636 400 nm (D_{va}). In addition, by using the IMPROVE method, we found that the
637 observed PM_1 components were able to reproduce ~44% of the light extinction during

this study.

PMF analyses resolved four OA factors, e.g., HOA, COA, SV-OOA and LV-OOA. Mass spectral profiles of these factors agree very well with the corresponding factors identified at other locations. The springtime OA showed no influences from biomass burning emissions. On average, the OA is dominated by SOA (55.5%), but POA appeared to be more important when the OA mass loadings are high, and can be dominant in early morning and evening. Diurnal cycle of SV-OOA varied similarly to that of nitrate, reflecting its semi-volatile behavior. Diurnal variations of LV-OOA showed great resemblance to that of sulfate~~, indicating its formation was mainly from photochemical oxidation, as well~~. The bivariate polar plots indicate that SV-OOA was formed locally, and the Van Krevelen diagram further suggests a transformation from~~pathway of~~ SV-OOA to LV-OOA in Nanjing~~ probably via the addition of carboxylic acid~~. Generally, our highly time-resolved SP-AMS measurement results may offer useful insights into the aerosol chemistry, and have important implications for the PM control and reduction in this densely populated region.

Acknowledgements

This work was supported by the Natural Science Foundation of China (Grant Nos. 21407079 and 91544220), the Jiangsu Natural Science Foundation (BK20150042), the Jiangsu Provincial Specially-Appointed Professors Foundation~~, the Jiangsu Innovation and Entrepreneurship Program, the Startup Foundation for Introducing Talent of NUIST (2014r064)~~, ~~and~~ the LAPC Open Fund (LAPC-KF-2014-06), and the project funded by the Priority Academic Program Development of Jiangsu Higher Education Institutions (PAPD).~~.~~ M. Chen ~~also~~ acknowledges the support from the Natural Science Foundation of China (Grant Nos. 21577065 and 91543115), ~~the Commonweal Program of Environment Protection Department of China (201409027-05),~~ and the International ST Cooperation Program of China (2014DFA90780). J. Wang also acknowledges the financial support from China Scholarship Council, and the innovative project for graduate student of Jiangsu

Province. The authors thank Nanjing Environmental Monitoring Center for the supporting data, and the helps from ~~Shun Ge,~~ Ling Li, Yanan He, Hui Chen and Yangzhou Wu during the campaign and preparation of the manuscript.

References

Aiken, A. C., Decarlo, P. F., Kroll, J. H., Worsnop, D. R., Huffman, J. A., Docherty, K. S., Ulbrich, I. M., Mohr, C., Kimmel, J. R., Sueper, D., Sun, Y., Zhang, Q., Trimborn, A., Northway, M., Ziemann, P. J., Canagaratna, M. R., Onasch, T. B., Alfarra, M. R., Prevot, A. S. H., Dommen, J., Duplissy, J., Metzger, A., Baltensperger, U., and Jimenez, J. L.: O/C and OM/OC ratios of primary, secondary, and ambient organic aerosols with high-resolution time-of-flight aerosol mass spectrometry, Environ. Sci. Technol., 42, 4478-4485, 10.1021/Es703009q, 2008.

Alfarra, M. R., Prevot, A. S. H., Szidat, S., Sandradewi, J., Weimer, S., Lanz, V. A., Schreiber, D., Mohr, M., and Baltensperger, U.: Identification of the Mass Spectral Signature of Organic Aerosols from Wood Burning Emissions, Environ. Sci. Technol., 41, 5770-5777, 10.1021/es062289b, 2007.

Allan, J. D., Williams, P. I., Morgan, W. T., Martin, C. L., Flynn, M. J., Lee, J., Nemitz, E., Phillips, G. J., Gallagher, M. W., and Coe, H.: Contributions from transport, solid fuel burning and cooking to primary organic aerosols in two UK cities, Atmos. Chem. Phys., 10, 647-668, 10.5194/acp-10-647-2010, 2010.

Canagaratna, M. R., Jayne, J. T., Ghertner, D. A., Herndon, S., Shi, Q., Jimenez, J. L., Silva, P. J., Williams, P., Lanni, T., Drewnick, F., Demerjian, K. L., Kolb, C. E., and Worsnop, D. R.: Chase studies of particulate emissions from in-use New York City vehicles, Aerosol Sci. Tech., 38, 555-573, 10.1080/02786820490465504, 2004.

Canagaratna, M. R., Jayne, J. T., Jimenez, J. L., Allan, J. D., Alfarra, M. R., Zhang, Q., Onasch, T. B., Drewnick, F., Coe, H., Middlebrook, A., Delia, A., Williams, L. R., Trimborn, A. M., Northway, M. J., DeCarlo, P. F., Kolb, C. E., Davidovits, P., and Worsnop, D. R.: Chemical and microphysical characterization of ambient aerosols with the aerodyne aerosol mass spectrometer, Mass Spectrom. Rev., 26, 185-222, 10.1002/Mas.20115, 2007.

Canagaratna, M. R., Jimenez, J. L., Kroll, J. H., Chen, Q., Kessler, S. H., Massoli, P., Hildebrandt Ruiz, L., Fortner, E., Williams, L. R., Wilson, K. R., Surratt, J. D., Donahue, N. M., Jayne, J. T., and Worsnop, D. R.: Elemental ratio measurements of organic compounds using aerosol mass spectrometry: characterization, improved calibration, and implications, Atmos. Chem. Phys., 15, 253-272, 10.5194/acp-15-253-2015, 2015.

Cao, J. J., Xu, H. M., Xu, Q., Chen, B. H., and Kan, H. D.: Fine Particulate Matter Constituents and Cardiopulmonary Mortality in a Heavily Polluted Chinese City, Environ. Health Persp., 120, 373-378, 10.1289/ehp.1103671, 2012.

Carslaw, D. C., and Beevers, S. D.: Characterising and understanding emission sources using bivariate polar plots and k-means clustering, Environ. Model. Soft., 40, 325-329, 10.1016/j.envsoft.2012.09.005, 2013.

Carslaw, K. S., Boucher, O., Spracklen, D. V., Mann, G. W., Rae, J. G. L., Woodward, S., and

708 Kulmala, M.: A review of natural aerosol interactions and feedbacks within the Earth system,
709 Atmos. Chem. Phys., 10, 1701-1737, 10.5194/acp-10-1701-2010, 2010.

710 Chen, C., Sun, Y. L., Xu, W. Q., Du, W., Zhou, L. B., Han, T. T., Wang, Q. Q., Fu, P. Q., Wang,
711 Z. F., Gao, Z. Q., Zhang, Q., and Worsnop, D. R.: Characteristics and sources of submicron
712 aerosols above the urban canopy (260 m) in Beijing, China, during the 2014 APEC summit,
713 Atmos. Chem. Phys., 15, 12879-12895, 10.5194/acp-15-12879-2015, 2015.

714 Collier, S., Zhou, S., Kuwayama, T., Forestieri, S., Brady, J., Zhang, M., Kleeman, M., Cappa,
715 C., Bertram, T., and Zhang, Q.: Organic PM Emissions from Vehicles: Composition, O/C
716 Ratio, and Dependence on PM Concentration, Aerosol Sci. Tech., 49, 86-97,
717 10.1080/02786826.2014.1003364, 2015.

718 DeCarlo, P. F., Slowik, J. G., Worsnop, D. R., Davidovits, P., and Jimenez, J. L.: Particle
719 morphology and density characterization by combined mobility and aerodynamic diameter
720 measurements. Part 1: Theory, Aerosol Sci. Tech., 38, 1185-1205,
721 10.1080/02786820590928897, 2004.

722 DeCarlo, P. F., Kimmel, J. R., Trimborn, A., Northway, M. J., Jayne, J. T., Aiken, A. C., Gonin,
723 M., Fuhrer, K., Horvath, T., Docherty, K. S., Worsnop, D. R., and Jimenez, J. L.:
724 Field-deployable, high-resolution, time-of-flight aerosol mass spectrometer, Anal. Chem., 78,
725 8281-8289, 10.1021/Ac061249n, 2006.

726 Denjean, C., Formenti, P., Picquet-Varrault, B., Pangui, E., Zapf, P., Katrib, Y., Giorio, C.,
727 Tapparo, A., Monod, A., Temime-Roussel, B., Decorse, P., Mangeney, C., and Doussin, J. F.:
728 Relating hygroscopicity and optical properties to chemical composition and structure of
729 secondary organic aerosol particles generated from the ozonolysis of α-pinene, Atmos. Chem.
730 Phys., 15, 3339-3358, 10.5194/acp-15-3339-2015, 2015.

731 Dong, H. B., Zeng, L. M., Hu, M., Wu, Y. S., Zhang, Y. H., Slanina, J., Zheng, M., Wang, Z.
732 F., and Jansen, R.: Technical Note: The application of an improved gas and aerosol collector
733 for ambient air pollutants in China, Atmos. Chem. Phys., 12, 10519-10533,
734 10.5194/acp-12-10519-2012, 2012.

735 Drewnick, F., Hings, S. S., DeCarlo, P., Jayne, J. T., Gonin, M., Fuhrer, K., Weimer, S.,
736 Jimenez, J. L., Demerjian, K. L., Borrmann, S., and Worsnop, D. R.: A new time-of-flight
737 aerosol mass spectrometer (TOF-AMS) - Instrument description and first field deployment,
738 Aerosol Sci. Tech., 39, 637-658, 10.1080/02786820500182040, 2005.

739 Du, W., Sun, Y. L., Xu, Y. S., Jiang, Q., Wang, Q. Q., Yang, W., Wang, F., Bai, Z. P., Zhao, X.
740 D., and Yang, Y. C.: Chemical characterization of submicron aerosol and particle growth
741 events at a national background site (3295 m a.s.l.) on the Tibetan Plateau, Atmos. Chem.
742 Phys., 15, 10811-10824, 10.5194/acp-15-10811-2015, 2015.

743 Duplissy, J., DeCarlo, P. F., Dommen, J., Alfarra, M. R., Metzger, A., Barmpadimos, I., Prevot,
744 A. S. H., Weingartner, E., Tritscher, T., Gysel, M., Aiken, A. C., Jimenez, J. L., Canagaratna,

745 M. R., Worsnop, D. R., Collins, D. R., Tomlinson, J., and Baltensperger, U.: Relating
746 hygroscopicity and composition of organic aerosol particulate matter, Atmos. Chem. Phys., 11,
747 1155-1165, 10.5194/acp-11-1155-2011, 2011.

748 Fröhlich, R., Cubison, M. J., Slowik, J. G., Bukowiecki, N., Prévôt, A. S. H., Baltensperger,
749 U., Schneider, J., Kimmel, J. R., Gonin, M., Rohner, U., Worsnop, D. R., and Jayne, J. T.: The
750 ToF-ACSM: a portable aerosol chemical speciation monitor with TOFMS detection, Atmos.
751 Meas. Tech., 6, 3225-3241, 10.5194/amt-6-3225-2013, 2013.

752 Fu, Q. Y., Zhuang, G. S., Wang, J., Xu, C., Huang, K., Li, J., Hou, B., Lu, T., and Streets, D.
753 G.: Mechanism of formation of the heaviest pollution episode ever recorded in the Yangtze
754 River Delta, China, Atmos. Environ., 42, 2023-2036, 10.1016/j.atmosenv.2007.12.002, 2008.

755 Ge, X., Zhang, Q., Sun, Y., Ruehl, C. R., and Setyan, A.: Effect of aqueous-phase processing
756 on aerosol chemistry and size distributions in Fresno, California, during wintertime, Environ.
757 Chem., 9, 221-235, 10.1071/EN11168, 2012a.

758 Ge, X. L., Setyan, A., Sun, Y., and Zhang, Q.: Primary and secondary organic aerosols in
759 Fresno, California during wintertime: Results from high resolution aerosol mass spectrometry,
760 J. Geophys. Res. - Atmos., 117, D19301, 10.1029/2012jd018026, 2012b.

761 Ghan, S. J., and Schwartz, S. E.: Aerosol properties and processes: A path from field and
762 laboratory measurements to global climate models, Bull. Am. Meteorol. Soc., 88, 1059-1083,
763 10.1175/bams-88-7-1059, 2007.

764 Han, T., Xu, W., Chen, C., Liu, X., Wang, Q., Li, J., Zhao, X., Du, W., Wang, Z., and Sun, Y.:
765 Chemical apportionment of aerosol optical properties during the Asia-Pacific Economic
766 Cooperation summit in Beijing, China, J. Geophys. Res. - Atmos., 120, 12,281-212,295,
767 10.1002/2015JD023918, 2015.

768 He, L. Y., Huang, X.-F., Xue, L., Hu, M., Lin, Y., Zheng, J., Zhang, R., and Zhang, Y.-H.:
769 Submicron aerosol analysis and organic source apportionment in an urban atmosphere in
770 Pearl River Delta of China using high-resolution aerosol mass spectrometry, J. Geophys. Res.
771 - Atmos., 116, D12304, 10.1029/2010jd014566, 2011.

772 Heald, C. L., Kroll, J. H., Jimenez, J. L., Docherty, K. S., DeCarlo, P. F., Aiken, A. C., Chen,
773 Q., Martin, S. T., Farmer, D. K., and Artaxo, P.: A simplified description of the evolution of
774 organic aerosol composition in the atmosphere, Geophys. Res. Lett., 37, L08803,
775 10.1029/2010gl042737, 2010.

776 Hu, J., Ying, Q., Wang, Y., and Zhang, H.: Characterizing multi-pollutant air pollution in
777 China: Comparison of three air quality indices, Environ. Int., 84, 17-25,
778 10.1016/j.envint.2015.06.014, 2015.

779 Hu, W. W., Hu, M., Yuan, B., Jimenez, J. L., Tang, Q., Peng, J. F., Hu, W., Shao, M., Wang,
780 M., Zeng, L. M., Wu, Y. S., Gong, Z. H., Huang, X. F., and He, L. Y.: Insights on organic

781 aerosol aging and the influence of coal combustion at a regional receptor site of central
782 eastern China, Atmos. Chem. Phys., 13, 10095-10112, 10.5194/acp-13-10095-2013, 2013.

783 Hu, X., Zhang, Y., Ding, Z. H., Wang, T. J., Lian, H. Z., Sun, Y. Y., and Wu, J. C.:
784 Bioaccessibility and health risk of arsenic and heavy metals (Cd, Co, Cr, Cu, Ni, Pb, Zn and
785 Mn) in TSP and $PM_{2.5}$ in Nanjing, China, Atmos. Environ., 57, 146-152,
786 10.1016/j.atmosenv.2012.04.056, 2012.

787 Huang, X., Xue, L., Tian, X.-D., Shao, W.-W., Sun, T.-L., Gong, Z.-H., Ju, W.-W., Jiang, B.,
788 Hu, M., and He, L.-Y.: Highly time-resolved carbonaceous aerosol characterization in Yangtze
789 River Delta of China: composition, mixing state and secondary formation, Atmos. Environ.,
790 10.1016/j.atmosenv.2012.09.059, 2012a.

791 Huang, X. F., He, L. Y., Hu, M., Canagaratna, M. R., Sun, Y., Zhang, Q., Zhu, T., Xue, L.,
792 Zeng, L. W., Liu, X. G., Zhang, Y. H., Jayne, J. T., Ng, N. L., and Worsnop, D. R.: Highly
793 time-resolved chemical characterization of atmospheric submicron particles during 2008
794 Beijing Olympic Games using an Aerodyne High-Resolution Aerosol Mass Spectrometer,
795 Atmos. Chem. Phys., 10, 8933-8945, 10.5194/acp-10-8933-2010, 2010.

796 Huang, X. F., He, L. Y., Hu, M., Canagaratna, M. R., Kroll, J. H., Ng, N. L., Zhang, Y. H., Lin,
797 Y., Xue, L., Sun, T. L., Liu, X. G., Shao, M., Jayne, J. T., and Worsnop, D. R.:
798 Characterization of submicron aerosols at a rural site in Pearl River Delta of China using an
799 Aerodyne High-Resolution Aerosol Mass Spectrometer, Atmos. Chem. Phys., 11, 1865-1877,
800 10.5194/acp-11-1865-2011, 2011.

801 Huang, X. F., He, L. Y., Xue, L., Sun, T. L., Zeng, L. W., Gong, Z. H., Hu, M., and Zhu, T.:
802 Highly time-resolved chemical characterization of atmospheric fine particles during 2010
803 Shanghai World Expo, Atmos. Chem. Phys., 12, 4897-4907, 10.5194/acp-12-4897-2012,
804 2012b.

805 Jayne, J. T., Leard, D. C., Zhang, X., Davidovits, P., Smith, K. A., Kolb, C. E., and Worsnop,
806 D. R.: Development of an Aerosol Mass Spectrometer for Size and Composition Analysis of
807 Submicron Particles, Aerosol Sci. Tech., 33, 49 - 70, 10.1016/S0021-8502(98)00158-X, 2000.

808 Jiang, Q., Sun, Y. L., Wang, Z., and Yin, Y.: Aerosol composition and sources during the
809 Chinese Spring Festival: fireworks, secondary aerosol, and holiday effects, Atmos. Chem.
810 Phys., 15, 6023-6034, 10.5194/acp-15-6023-2015, 2015.

811 Jimenez, J. L., Jayne, J. T., Shi, Q., Kolb, C. E., Worsnop, D. R., Yourshaw, I., Seinfeld, J. H.,
812 Flagan, R. C., Zhang, X. F., Smith, K. A., Morris, J. W., and Davidovits, P.: Ambient aerosol
813 sampling using the Aerodyne Aerosol Mass Spectrometer, J. Geophys. Res. - Atmos., 108,
814 8425, 10.1029/2001jd001213, 2003.

815 Jimenez, J. L., Canagaratna, M. R., Donahue, N. M., Prevot, A. S. H., Zhang, Q., Kroll, J. H.,
816 DeCarlo, P. F., Allan, J. D., Coe, H., Ng, N. L., Aiken, A. C., Docherty, K. S., Ulbrich, I. M.,
817 Grieshop, A. P., Robinson, A. L., Duplissy, J., Smith, J. D., Wilson, K. R., Lanz, V. A.,

Hueglin, C., Sun, Y. L., Tian, J., Laaksonen, A., Raatikainen, T., Rautiainen, J., Vaattovaara, P., Ehn, M., Kulmala, M., Tomlinson, J. M., Collins, D. R., Cubison, M. J., Dunlea, E. J., Huffman, J. A., Onasch, T. B., Alfarra, M. R., Williams, P. I., Bower, K., Kondo, Y., Schneider, J., Drewnick, F., Borrmann, S., Weimer, S., Demerjian, K., Salcedo, D., Cottrell, L., Griffin, R., Takami, A., Miyoshi, T., Hatakeyama, S., Shimono, A., Sun, J. Y., Zhang, Y. M., Dzepina, K., Kimmel, J. R., Sueper, D., Jayne, J. T., Herndon, S. C., Trimborn, A. M., Williams, L. R., Wood, E. C., Middlebrook, A. M., Kolb, C. E., Baltensperger, U., and Worsnop, D. R.: Evolution of organic aerosols in the atmosphere, Science, 326, 1525-1529, 10.1126/science.1180353, 2009.

Kong, S. F., Li, L., Li, X. X., Yin, Y., Chen, K., Liu, D. T., Yuan, L., Zhang, Y. J., Shan, Y. P., and Ji, Y. Q.: The impacts of firework burning at the Chinese Spring Festival on air quality: insights of tracers, source evolution and aging processes, Atmos. Chem. Phys., 15, 2167-2184, 10.5194/acp-15-2167-2015, 2015.

Kulmala, M., Lappalainen, H. K., Petäjä, T., Kurten, T., Kerminen, V. M., Viisanen, Y., Hari, P., Sorvari, S., Bäck, J., Bondur, V., Kasimov, N., Kotlyakov, V., Matvienko, G., Baklanov, A., Guo, H. D., Ding, A., Hansson, H. C., and Zilitinkevich, S.: Introduction: The Pan-Eurasian Experiment (PEEX) – multidisciplinary, multiscale and multicomponent research and capacity-building initiative, Atmos. Chem. Phys., 15, 13085-13096, 10.5194/acp-15-13085-2015, 2015.

Lee, A. K. Y., Hayden, K. L., Herckes, P., Leaitch, W. R., Liggio, J., Macdonald, A. M., and Abbatt, J. P. D.: Characterization of aerosol and cloud water at a mountain site during WACS 2010: secondary organic aerosol formation through oxidative cloud processing, Atmos. Chem. Phys., 12, 7103-7116, 10.5194/acp-12-7103-2012, 2012.

Lee, B. P., Li, Y. J., Yu, J. Z., Louie, P. K. K., and Chan, C. K.: Physical and chemical characterization of ambient aerosol by HR-ToF-AMS at a suburban site in Hong Kong during springtime 2011, J. Geophys. Res. - Atmos., 118, 8625-8639, 10.1002/jgrd.50658, 2013.

Li, Y. J., Lee, B. P., Su, L., Fung, J. C. H., and Chan, C. K.: Seasonal characteristics of fine particulate matter (PM) based on high-resolution time-of-flight aerosol mass spectrometric (HR-ToF-AMS) measurements at the HKUST Supersite in Hong Kong, Atmos. Chem. Phys., 15, 37-53, 10.5194/acp-15-37-2015, 2015.

Malm, W. C., and Day, D. E.: Estimates of aerosol species scattering characteristics as a function of relative humidity, Atmos. Environ., 35, 2845-2860, 10.1016/S1352-2310(01)00077-2, 2001.

Matthew, B. M., Middlebrook, A. M., and Onasch, T. B.: Collection Efficiencies in an Aerodyne Aerosol Mass Spectrometer as a Function of Particle Phase for Laboratory Generated Aerosols, Aerosol Sci.Tech., 42, 884-898, 10.1080/02786820802356797, 2008.

Middlebrook, A. M., Bahreini, R., Jimenez, J. L., and Canagaratna, M. R.: Evaluation of Composition-Dependent Collection Efficiencies for the Aerodyne Aerosol Mass Spectrometer

using Field Data, Aerosol Sci. Tech., 46, 258-271, 10.1080/02786826.2011.620041, 2012.

Mohr, C., DeCarlo, P. F., Heringa, M. F., Chirico, R., Slowik, J. G., Richter, R., Reche, C., Alastuey, A., Querol, X., Seco, R., Peñuelas, J., Jiménez, J. L., Crippa, M., Zimmermann, R., Baltensperger, U., and Prévôt, A. S. H.: Identification and quantification of organic aerosol from cooking and other sources in Barcelona using aerosol mass spectrometer data, Atmos. Chem. Phys., 12, 1649-1665, 10.5194/acp-12-1649-2012, 2012.

Mohr, C., DeCarlo, P. F., Heringa, M. F., Chirico, R., Richter, R., Crippa, M., Querol, X., Baltensperger, U., and Prévôt, A. S. H.: Spatial Variation of Aerosol Chemical Composition and Organic Components Identified by Positive Matrix Factorization in the Barcelona Region, Environ. Sci. Technol., 49, 10421-10430, 10.1021/acs.est.5b02149, 2015.

Ng, N. L., Canagaratna, M. R., Zhang, Q., Jimenez, J. L., Tian, J., Ulbrich, I. M., Kroll, J. H., Docherty, K. S., Chhabra, P. S., Bahreini, R., Murphy, S. M., Seinfeld, J. H., Hildebrandt, L., Donahue, N. M., DeCarlo, P. F., Lanz, V. A., Prevot, A. S. H., Dinar, E., Rudich, Y., and Worsnop, D. R.: Organic aerosol components observed in Northern Hemispheric datasets from Aerosol Mass Spectrometry, Atmos. Chem. Phys., 10, 4625-4641, 10.5194/acp-10-4625-2010, 2010.

Ng, N. L., Herndon, S. C., Trimborn, A., Canagaratna, M. R., Croteau, P. L., Onasch, T. B., Sueper, D., Worsnop, D. R., Zhang, Q., Sun, Y. L., and Jayne, J. T.: An Aerosol Chemical Speciation Monitor (ACSM) for Routine Monitoring of the Composition and Mass Concentrations of Ambient Aerosol, Aerosol Sci. Tech., 45, 770-784, 10.1080/02786826.2011.560211, 2011.

Onasch, T. B., Trimborn, A., Fortner, E. C., Jayne, J. T., Kok, G. L., Williams, L. R., Davidovits, P., and Worsnop, D. R.: Soot particle aerosol mass spectrometer: Development, validation, and initial application, Aerosol Sci. Tech., 46, 804-817, 10.1080/02786826.2012.663948, 2012.

Onasch, T. B., Fortner, E. C., Trimborn, A. M., Lambe, A. T., Tiwari, A. J., Marr, L. C., Corbin, J. C., Mensah, A. A., Williams, L. R., Davidovits, P., and Worsnop, D. R.: Investigations of SP-AMS Carbon Ion Distributions as a Function of Refractory Black Carbon Particle Type, Aerosol Sci. Tech. , 49, 409-422, 10.1080/02786826.2015.1039959, 2015.

Paatero, P., and Tapper, U.: Positive matrix factorization: A non-negative factor model with optimal utilization of error estimates of data values, Environmetrics, 5, 111-126, 10.1002/env.3170050203, 1994.

Pope, C. A., and Dockery, D. W.: Health Effects of Fine Particulate Air Pollution: Lines that Connect, J. Air Waste Manage., 56, 709-742, 10.1080/10473289.2006.10464485, 2006.

Pöschl, U.: Atmospheric Aerosols: Composition, Transformation, Climate and Health Effects, Angewandte Chemie International Edition, 44, 7520-7540, 10.1002/anie.200501122, 2005.

Qi, L., Zhang, Y., Ma, Y., Chen, M., Ge, X., Ma, Y., Zheng, J., Wang, Z., and Li, S.: Source identification of trace elements in the atmosphere during the second Asian Youth Games in Nanjing, China: Influence of control measures on air quality, Atmos. Pollut. Res., 7, 547-556, http://dx.doi.org/10.1016/j.apr.2016.01.003, 2016.

Seinfeld, J. H., and Pandis, S. N.: Atmospheric Chemistry and Physics: From Air Pollution to Climate Change, John Wiley & Sons, New York, 2006.

Setyan, A., Zhang, Q., Merkel, M., Knighton, W. B., Sun, Y., Song, C., Shilling, J. E., Onasch, T. B., Herndon, S. C., Worsnop, D. R., Fast, J. D., Zaveri, R. A., Berg, L. K., Wiedensohler, A., Flowers, B. A., Dubey, M. K., and Subramanian, R.: Characterization of submicron particles influenced by mixed biogenic and anthropogenic emissions using high-resolution aerosol mass spectrometry: results from CARES, Atmos. Chem. Phys., 12, 8131-8156, 10.5194/acp-12-8131-2012, 2012.

Shen, G. F., Yuan, S. Y., Xie, Y. N., Xia, S. J., Li, L., Yao, Y. K., Qiao, Y. Z., Zhang, J., Zhao, Q. Y., Ding, A. J., Li, B., and Wu, H. S.: Ambient levels and temporal variations of $PM_{2.5}$ and PM_{10} at a residential site in the mega-city, Nanjing, in the western Yangtze River Delta, China, J. Environ. Sci. Health., Part A, 49, 171-178, 10.1080/10934529.2013.838851, 2014.

Shen, X. J., Sun, J. Y., Zhang, X. Y., Zhang, Y. M., Zhang, L., Che, H. C., Ma, Q. L., Yu, X. M., Yue, Y., and Zhang, Y. W.: Characterization of submicron aerosols and effect on visibility during a severe haze-fog episode in Yangtze River Delta, China, Atmos. Environ., 120, 307-316, 10.1016/j.atmosenv.2015.09.011, 2015.

Sun, Y., Jiang, Q., Wang, Z., Fu, P., Li, J., Yang, T., and Yin, Y.: Investigation of the Sources and Evolution Processes of Severe Haze Pollution in Beijing in January 2013, J. Geophys. Res. - Atmos., 2014JD021641, 10.1002/2014JD021641, 2014.

Sun, Y. L., Zhang, Q., Schwab, J. J., Demerjian, K. L., Chen, W. N., Bae, M. S., Hung, H. M., Hogrefe, O., Frank, B., Rattigan, O. V., and Lin, Y. C.: Characterization of the sources and processes of organic and inorganic aerosols in New York city with a high-resolution time-of-flight aerosol mass apectrometer, Atmos. Chem. Phys., 11, 1581-1602, 10.5194/acp-11-1581-2011, 2011.

Sun, Y. L., Du, W., Wang, Q., Zhang, Q., Chen, C., Chen, Y., Chen, Z., Fu, P., Wang, Z., Gao, Z., and Worsnop, D. R.: Real-Time Characterization of Aerosol Particle Composition above the Urban Canopy in Beijing: Insights into the Interactions between the Atmospheric Boundary Layer and Aerosol Chemistry, Environ. Sci. Technol., 49, 11340-11347, 10.1021/acs.est.5b02373, 2015a.

Sun, Y. L., Wang, Z. F., Du, W., Zhang, Q., Wang, Q. Q., Fu, P. Q., Pan, X. L., Li, J., Jayne, J., and Worsnop, D. R.: Long-term real-time measurements of aerosol particle composition in Beijing, China: seasonal variations, meteorological effects, and source analysis, Atmos. Chem. Phys., 15, 10149-10165, 10.5194/acp-15-10149-2015, 2015b.

930 Sun, Y. L., Wang, Z., Wild, O., Xu, W., Chen, C., Fu, P., Du, W., Zhou, L., Zhang, Q., Han, T.,
931 Wang, Q., Pan, X., Zheng, H., Li, J., Guo, X., Liu, J., and Worsnop, D. R.: "APEC Blue":
932 Secondary Aerosol Reductions from Emission Controls in Beijing, Sci. Rep., 6, 20668,
933 10.1038/srep20668, 2016.

934 Tang, L., Yu, H., Ding, A., Zhang, Y., Qin, W., Wang, Z., Chen, W., Hua, Y., and Yang, X.:
935 Regional contribution to PM1 pollution during winter haze in Yangtze River Delta, China, Sci.
936 Total Environ., 541, 161-166, 10.1016/j.scitotenv.2015.05.058, 2016.

937 Ulbrich, I. M., Canagaratna, M. R., Zhang, Q., Worsnop, D. R., and Jimenez, J. L.:
938 Interpretation of organic components from Positive Matrix Factorization of aerosol mass
939 spectrometric data, Atmos. Chem. Phys., 9, 2891-2918, 10.5194/acp-9-2891-2009, 2009.

940 Wang, G. H., Niu, S. L., Liu, C., and Wang, L. S.: Identification of dicarboxylic acids and
941 aldehyde of PM_{10} and $PM_{2.5}$ aerosols in Nanjing, China, Atmos. Environ., 36, 1941-1950,
942 10.1016/s1352-2310(02)00180-2, 2002.

943 Wang, G. H., Wang, H., Yu, Y. J., Gao, S. X., Feng, J. F., Gao, S. T., and Wang, L. S.:
944 Chemical characterization of water-soluble components of PM_{10} and $PM_{2.5}$ atmospheric
945 aerosols in five locations of Nanjing, China, Atmos. Environ., 37, 2893-2902,
946 10.1016/s1352-2310(03)00271-1, 2003.

947 Wang, G. H., Kawamura, K., Xie, M. J., Hu, S. Y., Cao, J. J., An, Z. S., Waston, J. G., and
948 Chow, J. C.: Organic molecular compositions and size distributions of Chinese summer and
949 autumn aerosols from Nanjing: Characteristic haze event caused by wheat straw burning,
950 Environ. Sci. Technol., 43, 6493-6499, 10.1021/es803086g, 2009.

951 Wang, G. H., Chen, C. L., Li, J. J., Zhou, B. H., Xie, M. J., Hu, S. Y., Kawamura, K., and
952 Chen, Y.: Molecular composition and size distribution of sugars, sugar-alcohols and
953 carboxylic acids in airborne particles during a severe urban haze event caused by wheat straw
954 burning, Atmos. Environ., 45, 2473-2479, 10.1016/j.atmosenv.2011.02.045, 2011.

955 Wang, J., Onasch, T. B., Ge, X., Collier, S., Zhang, Q., Sun, Y., Yu, H., Chen, M., Prévôt, A. S.
956 H., and Worsnop, D. R.: Observation of Fullerene Soot in Eastern China, Environ. Sci.
957 Technol. Lett., 3, 121-126, 10.1021/acs.estlett.6b00044, 2016a.

958 Wang, Q., Sun, Y., Jiang, Q., Du, W., Sun, C., Fu, P., and Wang, Z.: Chemical composition of
959 aerosol particles and light extinction apportionment before and during the heating season in
960 Beijing, China, J. Geophys. Res. - Atmos., 120, 2015JD023871, 10.1002/2015JD023871,
961 2015.

962 Wang, Q., Zhao, J., Du, W., Ana, G., Wang, Z., Sun, L., Wang, Y., Zhang, F., Li, Z., Ye, X.,
963 and Sun, Y.: Characterization of submicron aerosols at a suburban site in central China, Atmos
964 Environ, 131, 115-123, http://dx.doi.org/10.1016/j.atmosenv.2016.01.054, 2016b.

965 Wexler, A. S., and Johnston, M. V.: What have we learned from highly time-resolved

966 measurements during EPA's Supersites program,and related studies?, J. Air Waste Manage.,
967 58, 303-319, 10.3155/1047-3289.58.2.303, 2008.

968 Xu, J., Zhang, Q., Chen, M., Ge, X., Ren, J., and Qin, D.: Chemical composition, sources, and
969 processes of urban aerosols during summertime in northwest China: insights from
970 high-resolution aerosol mass spectrometry, Atmos. Chem. Phys., 14, 12593-12611,
971 10.5194/acp-14-12593-2014, 2014.

972 Xu, W. Q., Sun, Y. L., Chen, C., Du, W., Han, T. T., Wang, Q. Q., Fu, P. Q., Wang, Z. F., Zhao,
973 X. J., Zhou, L. B., Ji, D. S., Wang, P. C., and Worsnop, D. R.: Aerosol composition, oxidation
974 properties, and sources in Beijing: results from the 2014 Asia-Pacific Economic Cooperation
975 summit study, Atmos. Chem. Phys., 15, 13681-13698, 10.5194/acp-15-13681-2015, 2015.

976 Yan, J., Chen, L., Lin, Q., Li, Z., Chen, H., and Zhao, S.: Chemical characteristics of
977 submicron aerosol particles during a long-lasting haze episode in Xiamen, China, Atmos.
978 Environ., 113, 118-126, 10.1016/j.atmosenv.2015.05.003, 2015.

979 Yang, H., Yu, J. Z., Ho, S. S. H., Xu, J. H., Wu, W. S., Wan, C. H., Wang, X. D., Wang, X. R.,
980 and Wang, L. S.: The chemical composition of inorganic and carbonaceous materials in $PM_{2.5}$
981 in Nanjing, China, Atmos. Environ., 39, 3735-3749, 10.1016/j.atmosenv.2005.03.010, 2005.

982 Yang, L.-X., Wang, D.-c., Cheng, S.-h., Wang, Z., Zhou, Y., Zhou, X.-h., and Wang, W.-x.:
983 Influence of meteorological conditions and particulate matter on visual range impairment in
984 Jinan, China, Sci. Total Environ., 383, 164-173, 10.1016/j.scitotenv.2007.04.042, 2007.

985 Yeung, M. C., Lee, B. P., Li, Y. J., and Chan, C. K.: Simultaneous HTDMA and
986 HR-ToF-AMS measurements at the HKUST Supersite in Hong Kong in 2011, J. Geophys.
987 Res. - Atmos., 2013JD021146, 10.1002/2013JD021146, 2014.

988 Young, D. E., Kim, H., Parworth, C., Zhou, S., Zhang, X., Cappa, C. D., Seco, R., Kim, S.,
989 and Zhang, Q.: Influences of emission sources and meteorology on aerosol chemistry in a
990 polluted urban environment: results from DISCOVER-AQ California, Atmos. Chem. Phys.,
991 16, 5427-5451, 10.5194/acp-16-5427-2016, 2016.

992 Yu, L., Smith, J., Laskin, A., Anastasio, C., Laskin, J., and Zhang, Q.: Chemical
993 characterization of SOA formed from aqueous-phase reactions of phenols with the triplet
994 excited state of carbonyl and hydroxyl radical, Atmos. Chem. Phys., 14, 13801-13816,
995 10.5194/acp-14-13801-2014, 2014.

996 Zhang, J. K., Sun, Y., Liu, Z. R., Ji, D. S., Hu, B., Liu, Q., and Wang, Y. S.: Characterization
997 of submicron aerosols during a month of serious pollution in Beijing, 2013, Atmos. Chem.
998 Phys., 14, 2887-2903, 10.5194/acp-14-2887-2014, 2014.

999 Zhang, J. K., Wang, L. L., Wang, Y. H., and Wang, Y. S.: Submicron aerosols during the
1000 Beijing Asia–Pacific Economic Cooperation conference in 2014, Atmos. Environ., 124, Part
1001 B, 224-231, 10.1016/j.scitotenv.2007.04.042, 2016a.

Zhang, Q., Alfarra, M. R., Worsnop, D. R., Allan, J. D., Coe, H., Canagaratna, M. R., and Jimenez, J. L.: Deconvolution and quantification of hydrocarbon-like and oxygenated organic aerosols based on aerosol mass spectrometry, Environ. Sci. Technol., 39, 4938-4952, 10.1021/Es048568l, 2005.

Zhang, Q., Jimenez, J. L., Canagaratna, M. R., Allan, J. D., Coe, H., Ulbrich, I., Alfarra, M. R., Takami, A., Middlebrook, A. M., Sun, Y. L., Dzepina, K., Dunlea, E., Docherty, K., DeCarlo, P. F., Salcedo, D., Onasch, T., Jayne, J. T., Miyoshi, T., Shimono, A., Hatakeyama, S., Takegawa, N., Kondo, Y., Schneider, J., Drewnick, F., Borrmann, S., Weimer, S., Demerjian, K., Williams, P., Bower, K., Bahreini, R., Cottrell, L., Griffin, R. J., Rautiainen, J., Sun, J. Y., Zhang, Y. M., and Worsnop, D. R.: Ubiquity and dominance of oxygenated species in organic aerosols in anthropogenically-influenced Northern Hemisphere midlatitudes, Geophys. Res. Lett., 34, L13801, 10.1029/2007gl029979, 2007a.

Zhang, Q., Jimenez, J. L., Worsnop, D. R., and Canagaratna, M.: A case study of urban particle acidity and its influence on secondary organic aerosol, Environ. Sci. Technol., 41, 3213-3219, 10.1021/Es061812j, 2007b.

Zhang, Q., Jimenez, J., Canagaratna, M., Ulbrich, I., Ng, N., Worsnop, D., and Sun, Y.: Understanding atmospheric organic aerosols via factor analysis of aerosol mass spectrometry: a review, Anal. Bioanal. Chem., 401, 3045-3067, 10.1007/s00216-011-5355-y, 2011.

Zhang, Y. J., Tang, L. L., Wang, Z., Yu, H. X., Sun, Y. L., Liu, D., Qin, W., Canonaco, F., Prévôt, A. S. H., Zhang, H. L., and Zhou, H. C.: Insights into characteristics, sources, and evolution of submicron aerosols during harvest seasons in the Yangtze River delta region, China, Atmos. Chem. Phys., 15, 1331-1349, 10.5194/acp-15-1331-2015, 2015.

Zhang, Y. J., Tang, L., Yu, H., Wang, Z., Sun, Y., Qin, W., Chen, W., Chen, C., Ding, A., Wu, J., Ge, S., Chen, C., and Zhou, H.-c.: Chemical composition, sources and evolution processes of aerosol at an urban site in Yangtze River Delta, China during wintertime, Atmos. Environ., 123, 339-349, 10.1016/j.atmosenv.2015.08.017, 2016b.

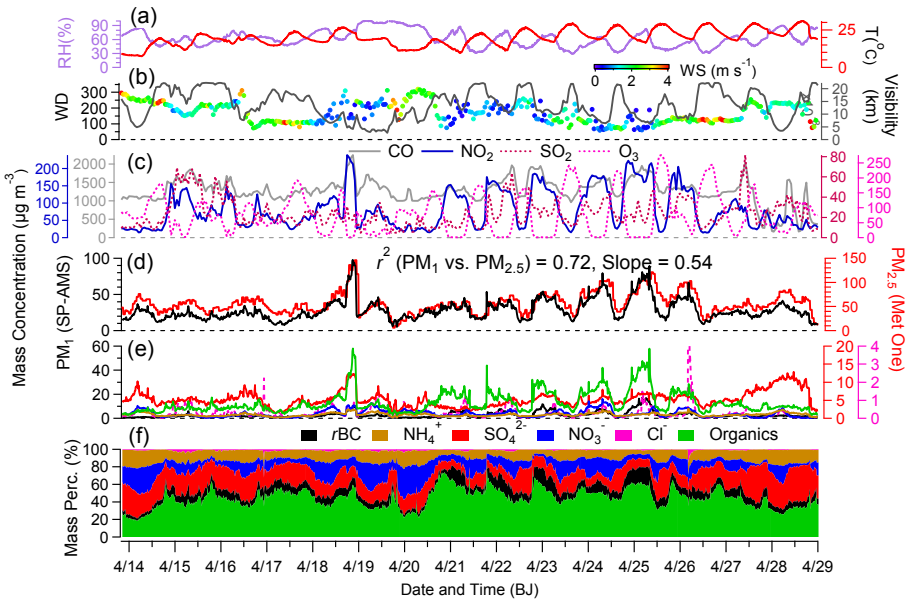

Figure 1. Time series of (a) relative humidity (RH) and temperature (T), (b) wind direction (WD) colored by wind speed (WS, m s^{-1}) and visibility (km), (c) mass concentrations of CO, NO_2, SO_2 and O_3 (hourly data), (d) mass concentrations of PM_1 measured by the SP-AMS, and $PM_{2.5}$ measured by the co-located Met One $PM_{2.5}$ analyzer, (e) mass concentrations of *r*BC, ammonium, sulfate, nitrate, chloride and organics, and (f) mass contributions (%) of the six PM_1 components (BJ, Beijing).

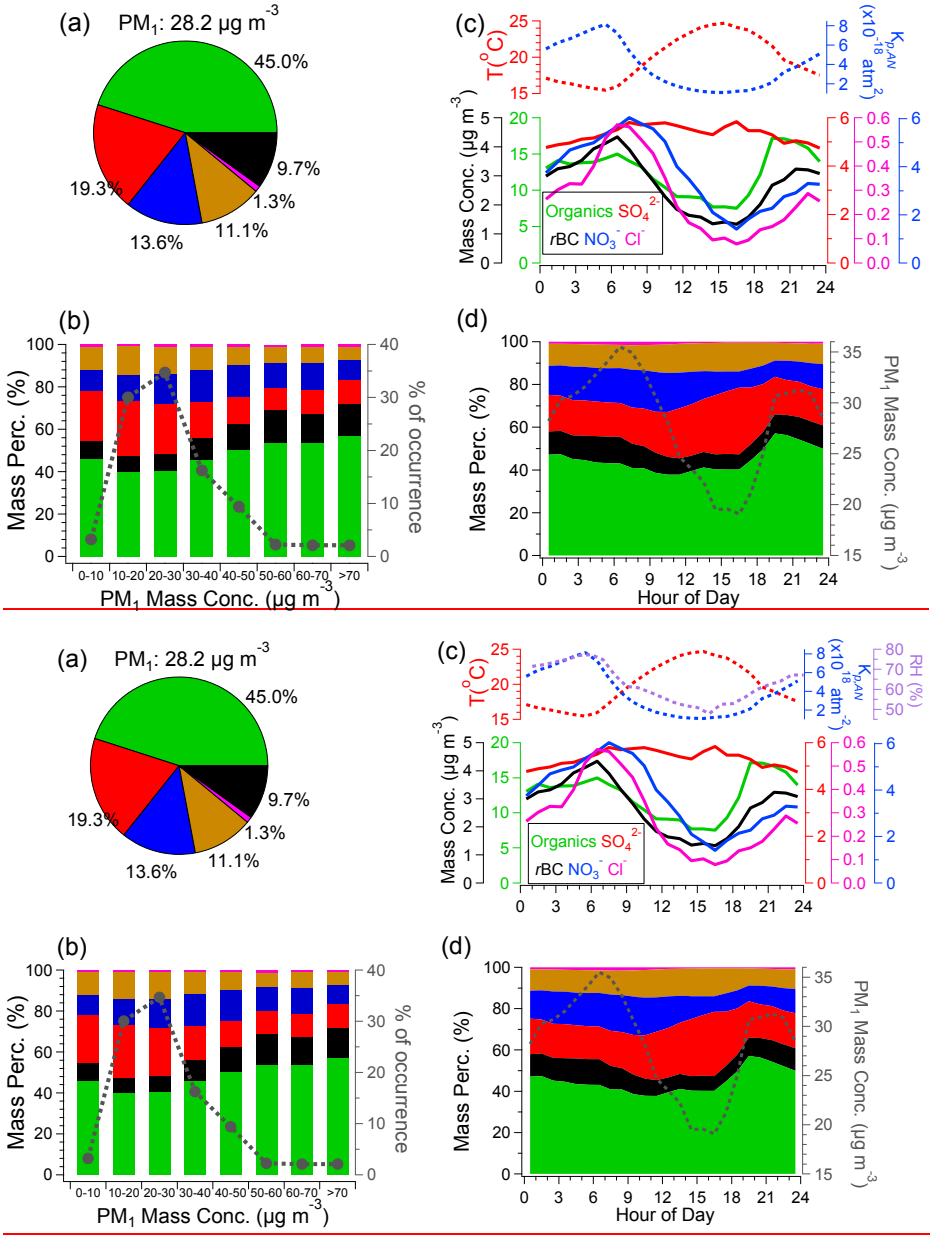

Figure 2. (a) Campaign-averaged mass contributions of organics, sulfate, nitrate, ammonium, chloride and *r*BC to the total PM_1, (b) mass percentages of the six PM_1 species (left *y*-axis) and, fractions of the number of data points to the total number of data points for PM_1 at different concentration bins (right *y*-axis), (c) diurnal patterns of mass concentrations of the major PM_1 species (bottom panel), temperature (top panel, left *y*-axis), relative humidity (RH) (top panel, right *y*-axis), and~~and~~ the equilibrium constant ($K_{p,AN}$) of NH_4NO_3 (top panel, right *y*-axis)

($K_{p,AN} = K_{p,AN}(298)exp\left\{a\left(\frac{298}{T}-1\right)+b\left[1+ln\left(\frac{298}{T}\right)-\frac{298}{T}\right]\right\}$, for reaction $NH_4NO_3(p) \leftrightarrow NH_3(g) + HNO_3(g)$. ~~$\leftrightarrow NH_4NO_3(p)$.~~ $K_{p,AN}(298)$ is the equilibrium constant at 298 K (3.36×10^{-16} atm^{-2}), a = 75.11, and b = -13.5 (Seinfeld and Pandis, 2006)), (d) diurnal variations of mass fractional contributions of the six PM_1 species (left *y*-axis), and the PM_1 mass concentrations (right *y*-axis).

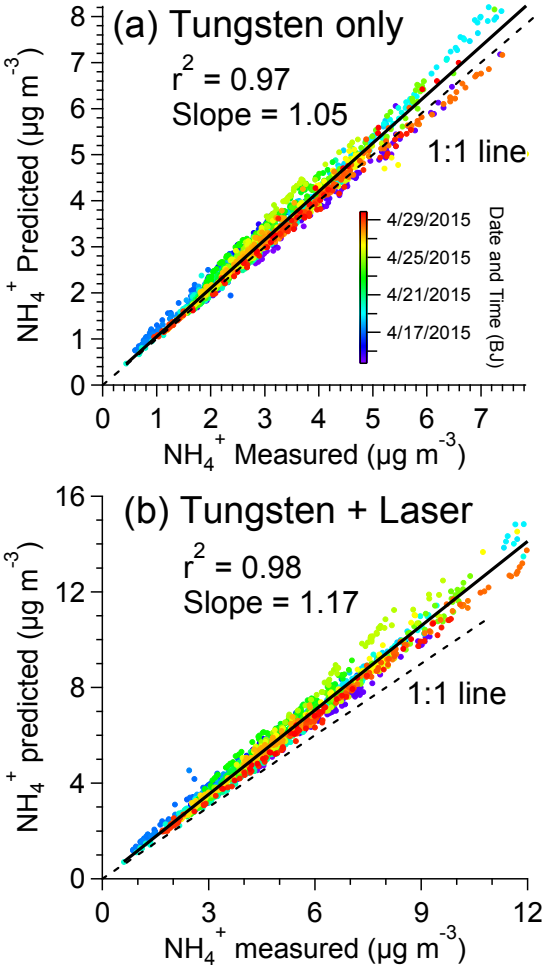

Figure 3. Scatter plots of the predicted NH_4^+ *vs.* measured NH_4^+ concentrations (colored by time), in the case of (a) tungsten vaporizer only, and (b) dual-vaporizers (tungsten + laser). The predicted values were calculated according to the formula: NH_4^+ predicted = $18\times(2\times SO_4^{2-}/96 + NO_3^-/62 + Cl^-/35.5)$ (Zhang et al., 2007b).

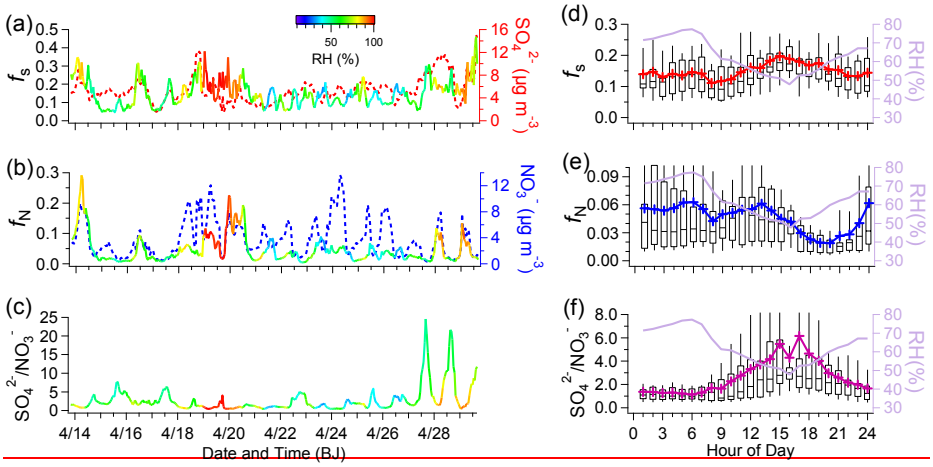

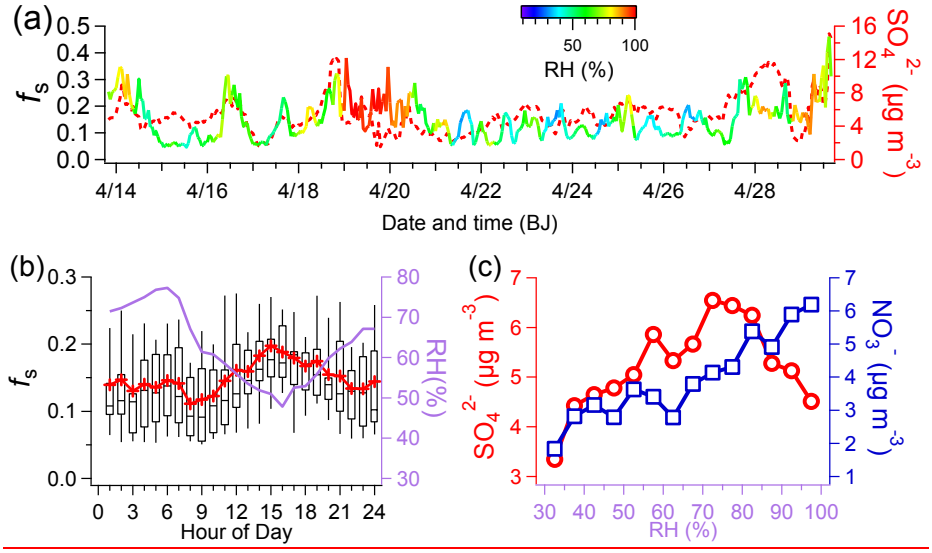

Figure 4. Time series of (a) sulfur oxidation ratio, $f_S = nSO_4^{2-}/(nSO_4^{2-} + nSO_2)$, and sulfate, (b) ~~nitrogen oxidation ratio, $f_N = nNO_3^-/(nNO_3^- + nNO_2)$, and nitrate, and (c) mass ratios of sulfate to nitrate (f_S, f_N and SO_4^{2-}/NO_3^- are colored by the relative humidity (RH) values),~~ diurnal variations of ~~(d)~~ f_S ~~, (e) f_N, and (f) SO_4^{2-}/NO_3^-~~ and RH (the lines and cross symbols indicate the mean values, the lines in the boxes indicate the median values, the upper and lower boundaries of the boxes indicate the 75th and 25th percentiles, and the whiskers above and below the boxes indicate the 90th and 10th percentiles), (c) Sulfate and nitrate concentrations *vs.* RH, the circles or squares represent the average concentrations within different RH bins (5% increment) for sulfate and nitrate, respectively.

1078

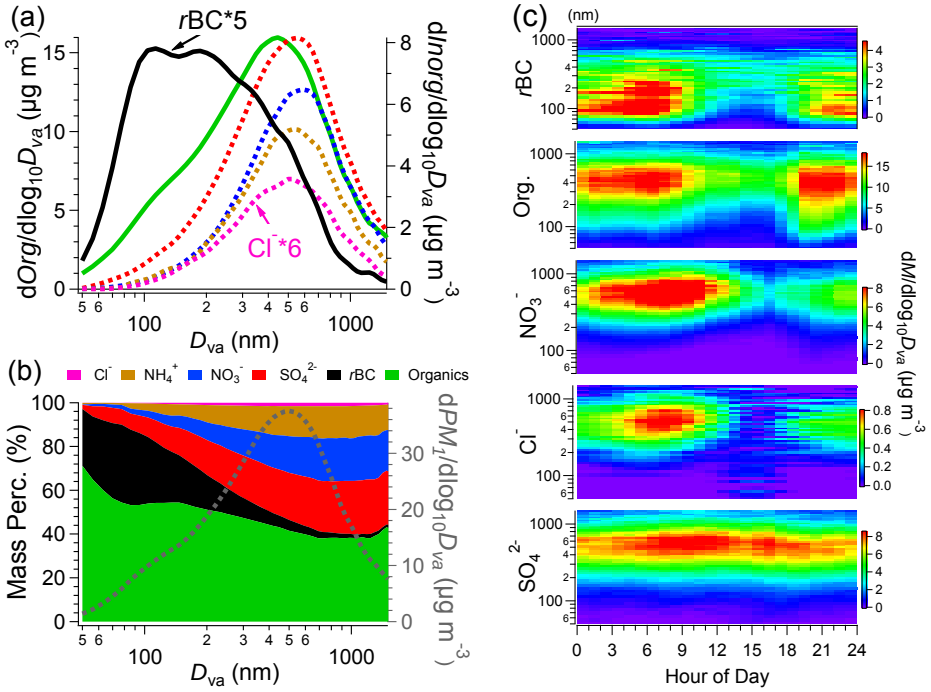

Figure 5. (a) Mass-based average size distributions of organics, *r*BC (left *y*-axis), sulfate, nitrate, chloride and ammonium (right *y*-axis) (D_{va}, vacuum aerodynamic diameter), (b) fractional contributions of the six PM_1 species as a function of particle size (left *y*-axis), and size distribution of total PM_1 (right *y*-axis), (c) diurnal profiles of the size distributions of *r*BC, organics, nitrate, chloride and sulfate.

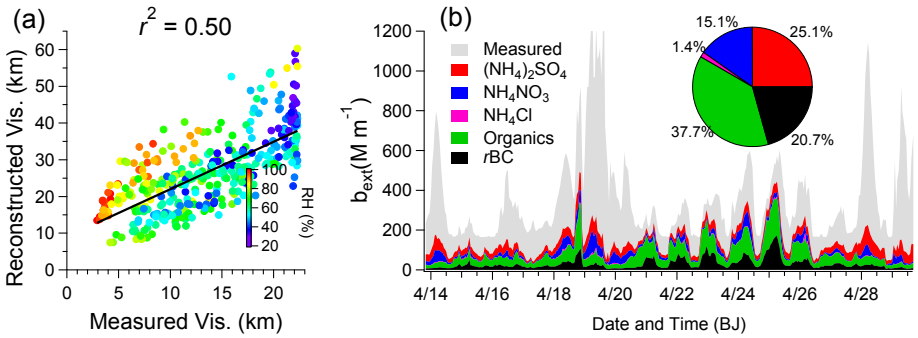

Figure 6. (a) Scatter plot of reconstructed *vs.* measured visibility (colored by RH), (b) light extinction coefficients derived from measured visibility (grey), and reconstructed from SP-AMS measured ammonium sulfate, ammonium nitrate, ammonium chloride, organics and *r*BC using the IMPROVE method. The inset pie shows the relative contributions of the five species to the light extinction of PM_1.

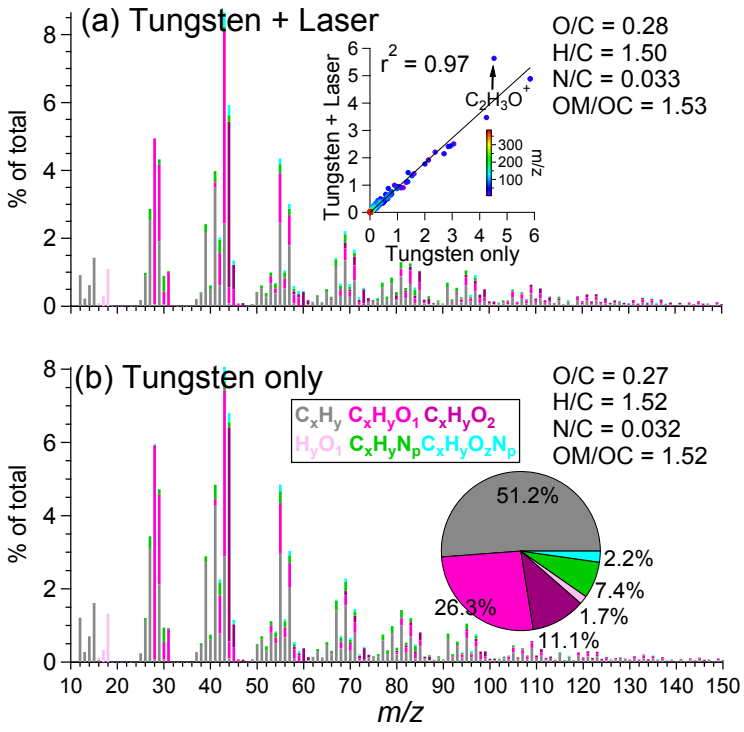

Figure 7. Campaign-averaged high resolution mass spectra of OA colored by six ion categories, in the case of (a) dual-vaporizers (tungsten + laser) (the inset scatter plot compares the spectral similarity between (a) and (b)), and (b) tungsten vaporizer only (the inset pie shows the relative contributions of six ion categories to the total OA).

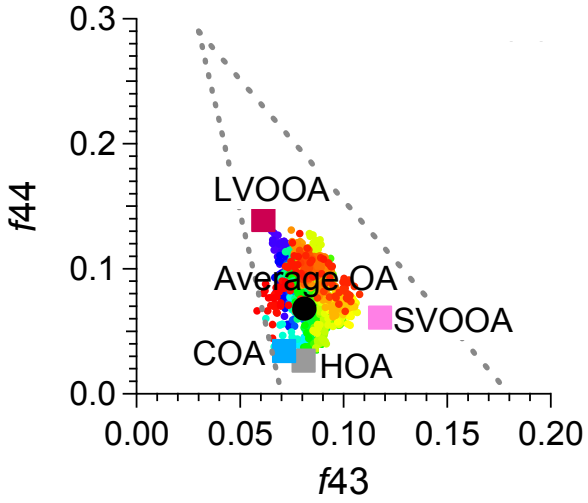

Figure 8. Triangle plot of *f*44 *vs.* *f*43 for all OA (colored by time), and the four OA factors identified by the PMF analyses.

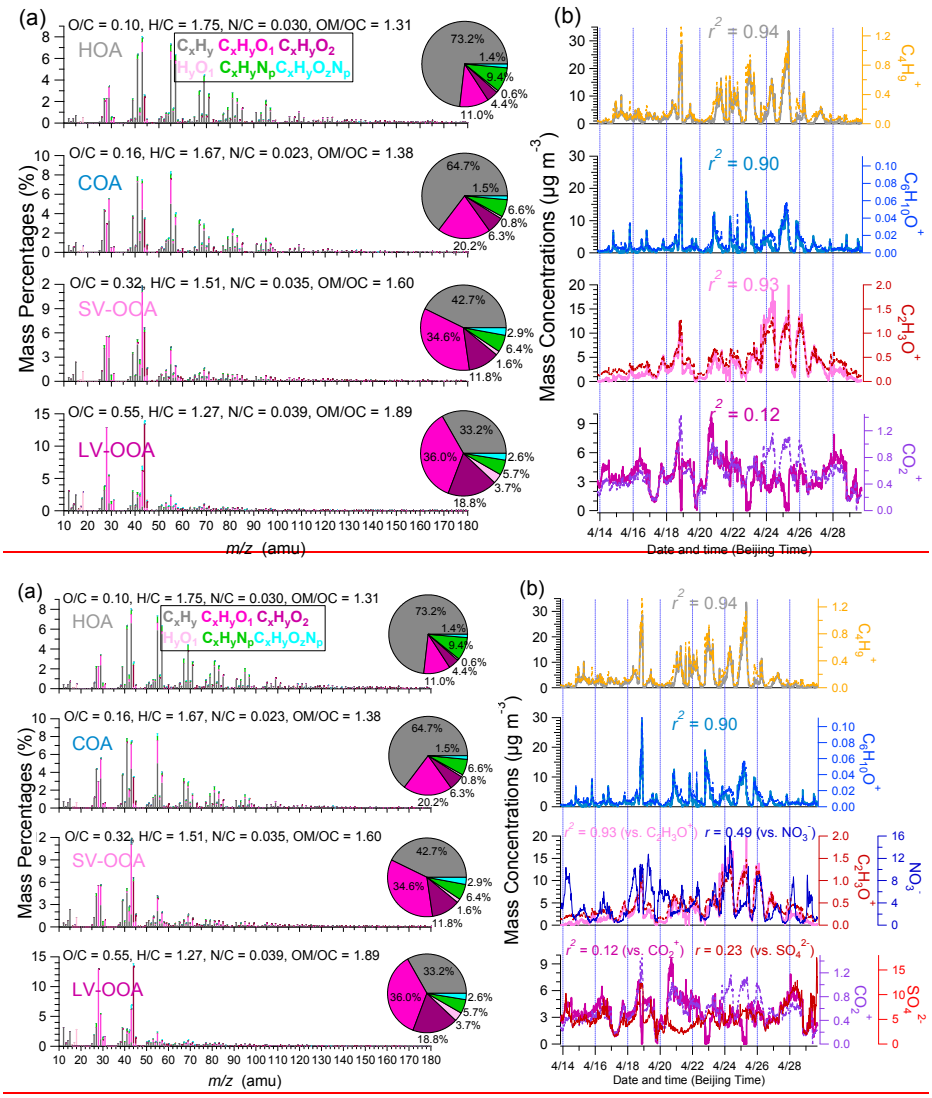

Figure 9. (a) High resolution mass spectra of hydrocarbon-like OA (HOA), cooking-related OA (COA), semi-volatile oxygenated OA (SV-OOA), and low volatility oxygenated OA (LV-OOA) colored by six ion categories (the four inset pies show the relative contributions of the six ion categories to the four OA factors, respectively), (b) time series of the four OA factors, ~~and~~ corresponding tracer ions, nitrate and sulfate. ~~.~~

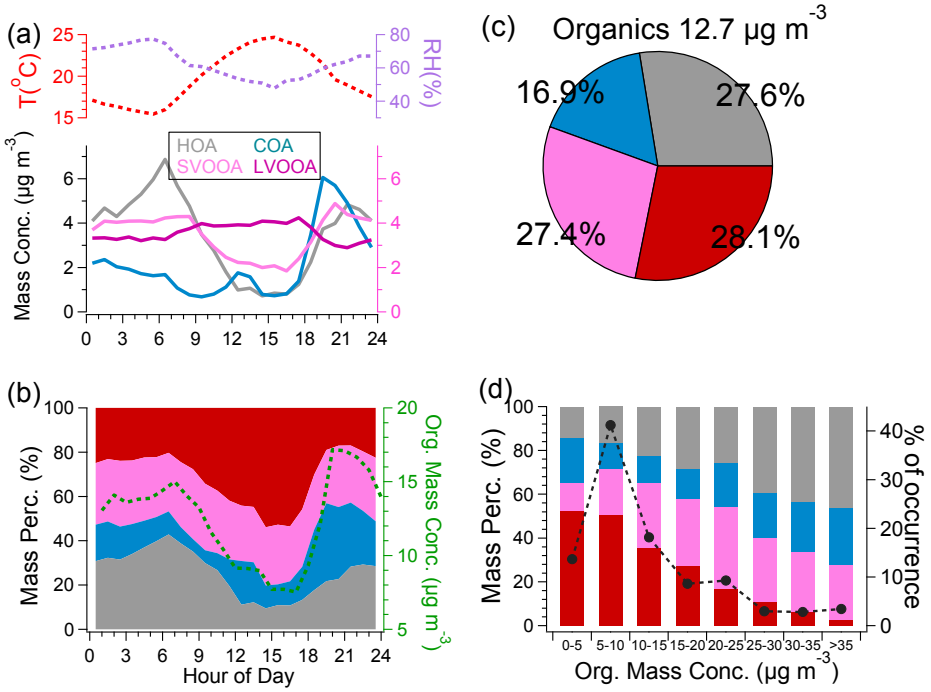

Figure 10. (a) Diurnal cycles of mass concentrations of the four OA factors (bottom panel), temperature (top panel, left *y*-axis) and RH (top panel, right *y*-axis), (b) diurnal variations of mass contributions of the four OA factors (left *y*-axis), and the total OA mass concentrations (right *y*-axis), (c) campaign-averaged mass contributions of the four OA factors to the total OA mass, and (d) mass contributions of the four OA factors (left *y*-axis), and the fractions of the number of data points to the total number of data points for the OA at different concentration ranges (right *y*-axis).

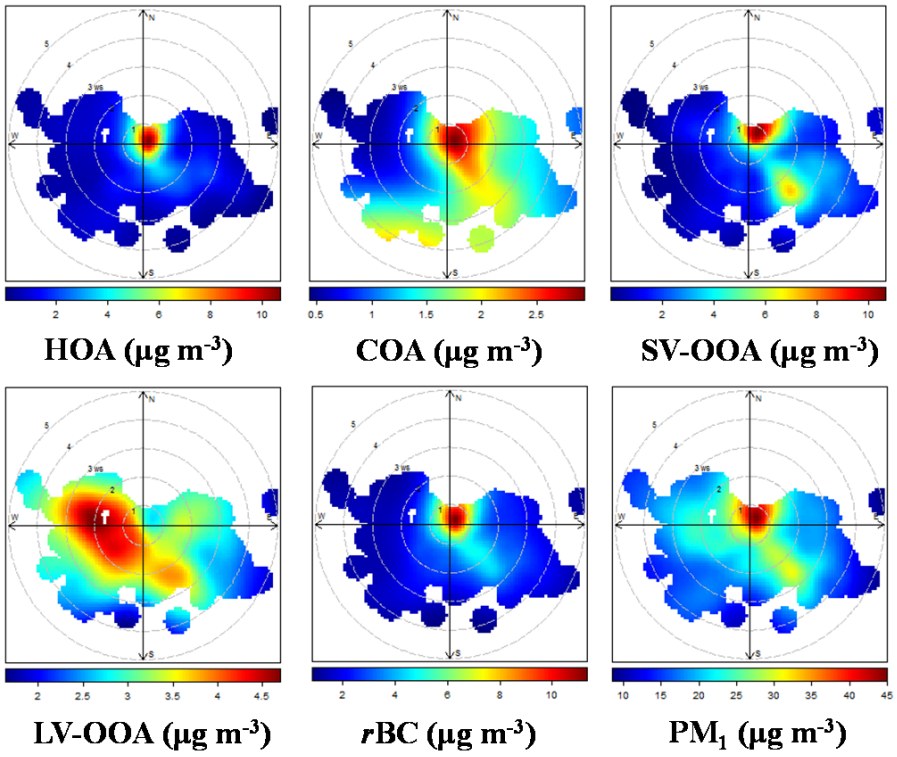

1131

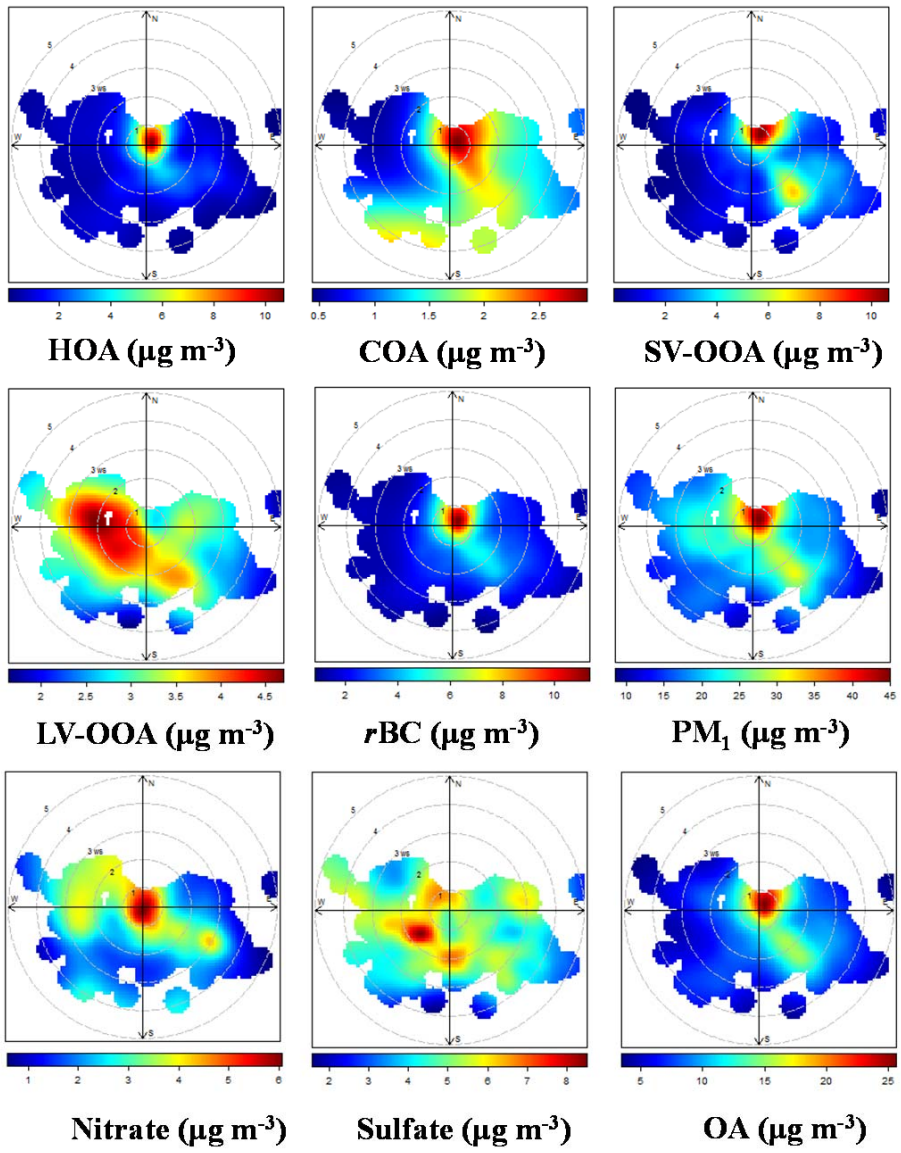

Figure 11. Bivariate polar plots of HOA, COA, SV-OOA, LV-OOA, *r*BC, ~~and~~ PM_1, nitrate, sulfate and the total OA (the color scale shows the concentration of each species, and the radical scale shows the wind speed that increases outward from the center).

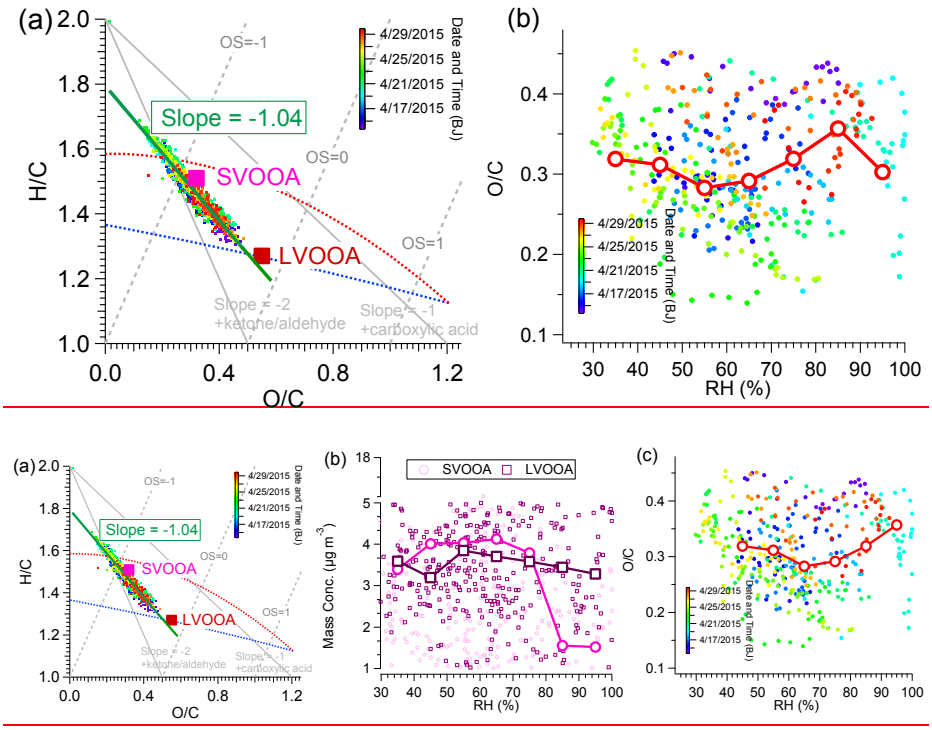

Figure 12. (a) Van Krevelen diagram of H/C *vs.* O/C ratios for all OA data colored by time, the blue and red dashed lines correspond to the right and left grey dashed lines in the *f*44 vs. f43 triangle plot of Fig. 8, the grey lines represents the addition of a particular functional group to an aliphatic carbon (Heald et al., 2010), (b) scatter plot of SVOOA and LVOOA mass concentrations *vs.* RH, the circles or squares represent the average mass concentrations within different RH bins (10% increment) for SVOOA and LVOOA, respectively, (c~~b~~) scatter plot of O/C *vs.* RH (colored by time), the circles represent~~s~~ the average O/C values within~~of~~ different~~the~~ RH bins (10% increment).~~—~~

Table 1. Correlation coefficients (Pearson's r^2) between the mass spectral profiles of the OA factors identified in this work with the corresponding factors identified in Beijing (2013 Winter) (Sun et al., 2015a), Lanzhou (2014 Summer) ((Xu et al., 2014)), and Fresno (2010 Winter) (Ge et al., 2012b).

Nanjing (2015 Spring)	High resolution MS (r^2)		
	Beijing (2013 Winter)	Lanzhou (2012 Summer)	Fresno (2010 Winter)*
HOA	0.92	0.90	0.98
COA	0.93	0.94	0.93
SV-OOA	0.68	0.75	0.90
LV-OOA	0.91	0.98	0.87
	Unit mass resolution MS (r^2)		
HOA	0.92	0.91	0.99
COA	0.96	0.96	0.95
SV-OOA	0.70	0.74	0.91
LV-OOA	0.90	0.98	0.89

*Note the Fresno (2010 Winter) study only identified one OOA factor, we thus compared both SV-OOA and LV-OOA in this study with it.

Table 2. Correlation coefficients (Pearson's *r*) between the time series of the four OA factors with the gas-phase species (hourly data) and other PM_1 components (15-min data), and the correlation coefficients between the diurnal data.

Pearson's *r*	Temp.(T)	CO	NO_2	SO_2	O_3	SO_4^{2-}	NO_3^-	Cl^-	*r*BC
	Hourly data					15-min data			
HOA	-0.14	0.71	0.77	0.13	-0.54	0.15	0.26	0.45	0.92
COA	0.11	0.50	0.58	-0.06	-0.22	0.19	0.07	0.08	0.61
SVOOA	0.19	0.41	0.70	0.14	-0.21	0.11	0.49	0.25	0.70
LVOOA	0.069	-0.2	-0.18	0.06	0.14	0.23	0.11	0.01	-0.22
	Diurnal data								
HOA	-0.94	0.86	0.86	0.66	-0.96	-0.35	0.72	0.82	0.99
COA	-0.15	0.28	0.59	-0.24	-0.24	-0.57	-0.33	-0.25	0.19
SVOOA	-0.85	0.86	0.94	0.58	-0.90	-0.51	0.53	0.61	0.89
LVOOA	0.76	-0.58	-0.83	-0.27	0.77	0.72	-0.26	-0.33	-0.75